Development of a Biocatalytic Aerobic Oxidation for the Manufacturing Route to Islatravir

Megan H. Shaw,†‡* Anna Fryszkowska,†‡* Oscar Alvizo,§ Ilana Attadgie,† Margie Borra-Garske,§ Paul N. Devine,† Da Duan,§ Shane T. Grosser,† Jacob H. Forstater,† Gregory J. Hughes,† Kevin M. Maloney,† Eric Margelefsky,† Keith A. Mattern,† Margaret T. Miller;† Christopher C. Nawrat,† Jovana Nazor,§ Peter Orth,‖ Claire M. Ouimet,¶ Sandra A. Robaire,† Serge Ruccolo,† Erica L. Schwalm,¶ Deeptak Verma,‖ Li Xiao‖; Victoria Zhang†

† Process Research & Development, Merck & Co., Inc., Rahway, NJ 07065, USA.

§ Codexis Inc., 200 Penobscot Drive, Redwood City, CA 94063, USA

‖ Discovery Chemistry, Merck & Co., Inc., Rahway, NJ 07065, USA.

¶ Analytical Research & Development, Merck & Co., Inc., Rahway, NJ 07065, USA.

KEYWORDS oxidation, biocatalysis, process development, drug manufacture, enzymatic cascades

ABSTRACT: Biocatalytic oxidations have the potential to address many synthetic chemistry challenges, enabling the selective synthesis of chiral intermediates such as carbonyl compounds, alcohols, or amines. The use of oxygen-dependent enzymes can dramatically reduce the environmental footprint of redox transformations at manufacturing scale. Here, as part of the biocatalytic cascade to an anti-HIV investigational drug islatravir **1**, we describe the development of an aerobic oxidation process delivering (*R*)-ethynylglyceraldehyde 3-phosphate **3** using an evolved galactose oxidase enzyme. Integrated enzyme and reaction engineering were critical for achieving a robust, high-yielding oxidation performed at pilot plant scale (>20 kg, 90% yield).

Scheme 1. Biocatalytic cascade to form islatravir **1**[1] from triol **2** with two potential sequences for accessing (*R*)-ethynylglyceraldehyde 3-phosphate **3**: oxidation 1st (bottom) and oxidation 2nd (top).

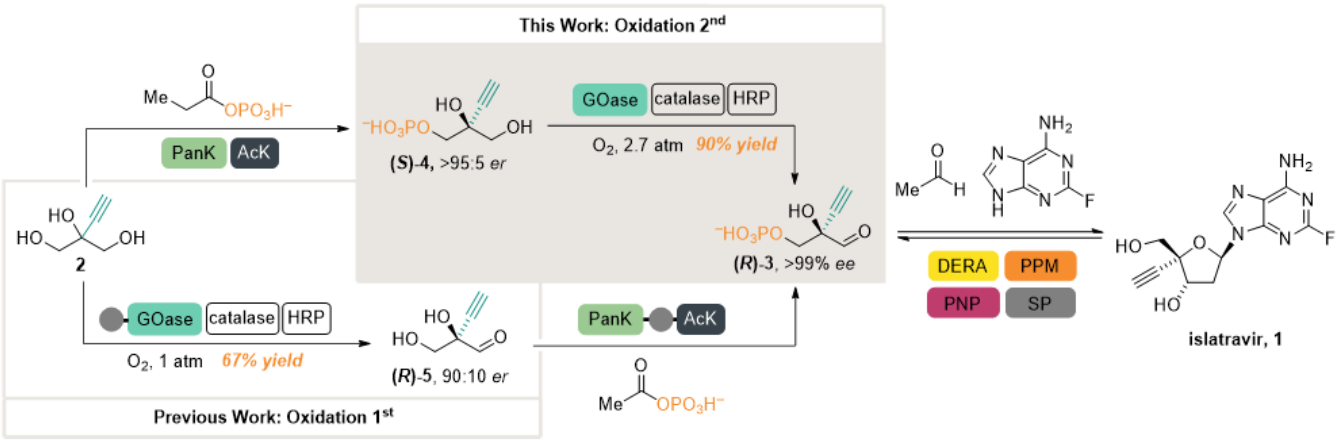

Footnote: Inversion of the phosphorylation and oxidation steps leads to an improved process to (*R*)-ethynylglyceraldehyde 3-phosphate (**3**), increasing the yield (for **2** to (***R***)-**3**) from 67% (bottom pathway) to 90% yield (top pathway). *Abbreviations:* PanK - evolved Pantothenate Kinase from *E. coli*; AcK – evolved Acetate Kinase from *Thermotoga maritima*; GOase – evolved Galactose Oxidase from *Fusarium graminearum*; HRP - Horseradish Peroxidase from *Amoracia rusticana*; DERA - evolved Deoxyribose-5-Phosphate Aldolase from *Shewanella halifaxensis;* PPM - evolved Phosphopentomutase from *E. coli*; PNP - evolved Purine Nucleoside Phosphorylase from *E. coli*; SP – evolved Sucrose Phosphorylase from *Alloscardovia omnicolens*; – Denotes an immobilized version of an enzyme.

1. Introduction

Expanding the synthetic chemists' toolbox to include enzyme catalysis offers opportunities for unparalleled selectivity, increased atom economy, and improved safety.[2] In vitro biocatalytic aerobic oxidations have potential as direct and sustainable methods for challenging transformations, such as selective C–H functionalization and aldehyde synthesis,[3] yet their industrial practice remains rare.[4–22] Naturally occurring oxygen-dependent enzymes seldom display the catalytic efficiency and robustness required for direct application in manufacturing processes. Consequently, their successful implementation at large scale requires protein engineering in parallel with process development to meet the demands of a manufacturing route.[23–26]

Islatravir (**1**, EFdA, or MK-8591) is an investigational drug for the treatment and prophylaxis of HIV that displays a novel mechanism of action as a nucleoside reverse transcriptase translocation inhibitor.[27] Recently, we disclosed a 9-enzyme cascade to prepare this nucleoside as a single stereoisomer, and this approach was demonstrated on gram-scale with 51% overall yield (Scheme 1, bottom).[1] The biocatalytic sequence from 2-ethynylglycerol (**2**)[28] proceeds *via* sequential oxidation and phosphorylation to give (*R*)-ethynylglyceraldehyde 3-phosphate (**3**), followed by a tandem aldol-glycosylation cascade to furnish islatravir (**1**). We aimed to translate this approach into a robust manufacturing process capable of providing >100 kg of active pharmaceutical ingredient (API).[29]

Herein, we describe the process development and pilot plant-scale demonstration of an aerobic oxidation of (*S*)-ethynylglycerol 1-phosphate (**4**) to (*R*)-ethynylglyceraldehyde 3-phosphate (**3**) using an engineered galactose oxidase (GOase) enzyme. We outline the strategic considerations relating to overall cascade efficiency that led to a switch in the step order for the oxidation-phosphorylation sequence (Scheme 1). We made critical advances through protein engineering, process development, and improvements in oxygen gas-liquid mass transfer, culminating in the demonstration of a robust, green, and sustainable enzymatic aerobic oxidation on multi-kilogram scale.

2. Results and Discussion

2.1 Cascade development considerations

Compared to previously published syntheses of islatravir (**1**), a biocatalytic cascade offers dramatically reduced step-count, improved atom economy, and simplified operations[1] (and references therein). However, the development of such an enzymatic approach presents several challenges with respect to process development.[29] Firstly, the lack of isolation points limits the opportunity for purity upgrades and imposes a requirement of high efficiency on each transformation. In this respect, the exquisite chemo-, regio- and stereoselectivity conferred by biocatalysts is crucial, enabling efficient conversion of the target intermediate within a complex reaction mixture. Secondly, having nine different enzymes involved in the cascade introduces the challenge of efficient protein management and purge to ensure delivery of high purity drug substance. Finally, a single-stream cascade demands a unified set of conditions for all the steps such that the components of prior step(s) do not hinder subsequent transformation(s). As a result, process optimization and enzyme engineering for the interconnected reactions must proceed concurrently, with data from each step informing overall process decisions.[25,29]

Phosphorylation and oxidation of 2-ethynylglycerol (**2**) to give (*R*)-glyceraldehyde 3-phosphate (**3**) could occur with the two steps proceeding in either order (Scheme 1, top *vs.* bottom sequence)[1]. Initially, we developed the "oxidation 1st" approach (Scheme 1, bottom), wherein the C2-stereogenic center was established *via* a desymmetrizing oxidation catalyzed by an evolved galactose oxidase variant $GOase_{Rd13BB}$.[1] Despite extensive rounds of directed evolution, high enzyme loading (20 wt%) was required to achieve full conversion. Additionally, the imperfect enantiopreference of $GOase_{Rd13BB}$ (90:10 *er*), coupled with deleterious formation of overoxidation byproducts, resulted in a moderate 67% yield of aldehyde **5**.

In contrast to the challenging evolution of the GOase enzyme, parallel protein engineering efforts focused on the pantothenate kinase (PanK) enzyme provided rapid improvements in enzyme activity for the phosphorylation of (*R*)-ethynylglyceraldehyde (**5**).[30] Notably, we also observed that the PanK enzyme possessed high activity towards triol **2**, displaying pro-*S* enantioselectivity (Scheme 1, top).[30] $PanK_{Rd4BB}$ catalyzed the formation of (*S*)-2-ethynylglycerol 1-phosphate (**4**) in quantitative yield and ≥95:5 *er*, leading to a 2–fold reduction in enzyme loading compared to the phosphorylation of aldehyde (*R*)-**5**. This motivated us to re-evaluate the activity of the GOase variants for the oxidation of (*S*)-2-ethynylglycerol 1-phosphate (**4**). While no product was detected with the early GOase variants,[1] $GOase_{Rd10BB}$-$GOase_{Rd13BB}$ catalyzed the formation of the desired aldehyde **3**, albeit in low yield (<17%) and at high enzyme loading (Scheme S 1). Evidently, over the course of directed evolution targeting oxidation of triol **2** to aldehyde (*R*)-**5**, the catalytic activity of the evolved GOase enzymes towards phosphorylated triol (*S*)-**4** had also increased.

This observation motivated us to re-evaluate the reaction sequence with inverted phosphorylation and oxidation steps to further improve the islatravir cascade and overall process. The "oxidation 2nd" sequence to aldehyde (*R*)-**3** (Scheme 1, top) offers several strategic advantages for the large-scale manufacture of islatravir: (*i*) high selectivity and yield when setting the C2-stereogenic center using the kinase (>95:5 *er*) *vs.* the oxidase-catalyzed desymmetrization (90:10 *er*); (*ii*) minimal byproduct formation in the PanK-catalyzed reaction on triol **2**[30] *vs.* significant overoxidation to carboxylic acid and dialdehyde byproducts in the GOase-catalyzed reaction[1]; (*iii*) reduced PanK enzyme loading due to the higher activity of the kinase towards triol **2** *vs.* aldehyde **5**;[30] and (*iv*) simplified directed evolution for the GOase enzyme focused solely on enzyme activity (for triol (*S*)-**4** to aldehyde (*R*)-**3**) rather than both activity and enantioselectivity (for triol **2** to aldehyde (*R*)-**5**). Consequently, we decided to continue the cascade development focusing on the "oxidation 2nd" approach.

2.2 Oxygen mass transfer and scalability considerations

At the outset of process development, we recognized that there would be two key challenges with respect to oxygen delivery. Firstly, GOase-catalyzed oxidation performance depends on the efficiency of oxygen mass transfer in the reaction system.[18,19] Specifically, for enzymatic aerobic oxidations, reaction kinetics can be limited by the low solubility of oxygen in aqueous buffers together with the high K_M for oxygen of certain enzyme classes (*i.e.* wild type galactose oxidase K_M >5 mM).[18,19] Moreover, reactors used in small molecule manufacturing plants are not typically designed to ensure efficient oxygen gas-liquid mass transfer. Therefore, careful consideration of process parameters (*e.g.,* temperature, pressure) and vessel configuration (*e.g.* geometry and mixing hydrodynamics) is required to achieve optimal oxygen delivery (Figure S 22).[31,32] Secondly, it is critical that efficient mass transfer can be replicated across scales from lab to plant settings. Initial studies focused on approximating the maximum oxygen mass transfer rate we could expect achieve at manufacturing scale, to allow process development studies to be carried out under relevant conditions.[31,32] The oxygen mass transfer rate is a combination of two factors: 1) k_La, a kinetic constant which describes how quickly a system reaches its maximum oxygen concentration, and 2) the thermodynamic driving force, which increases as the maximum theoretical concentration of oxygen in solution increases.[31–33] As the thermodynamic driving force is not scale dependent, our scalability/reproducibility studies focused on the kinetics of mass transfer, which is impacted by factors that change with scale, such as vessel dimensions, fill volume, and agitation rate.

We recently established methodology that enables characterization of the k_La in reaction vessels across scales,[31] which allowed us to study the impact of k_La on the oxidation reaction.[32] The oxidation enzymes were sufficiently active such that the kinetics of the biocatalytic oxidation reaction were dependent on the k_La in the reactor, with faster reaction rates achieved under higher k_La conditions. [31,32] We recognized that, while high k_La conditions would ensure optimal oxidation performance, it may not be possible to achieve high k_La in plant scale vessels. Consequently, we characterized a range of vessels from lab- to plant-scale at various reaction parameters (*e.g.,* agitation rate, air flow rate, reactor fill volume) and reactor configurations (*e.g.,* agitator height, impellor size and type, and baffle configuration) to yield a database of k_La values that could be achieved.[31] These studies guided our projection of the maximum achievable k_La in a small molecule manufacturing facility and consequently we targeted a k_La of 0.02 s^{-1} for process development studies. By profiling the kinetics of oxidation reactions performed in different vessels, we established that reproducible reaction performance could be achieved across scales (from 1 g lab-scale to multi-kilogram pilot plant-scale) provided that the reactions were performed at the same target k_La. These experiments provided us with confidence that process improvements validated at lab-scale would directly translate to improved performance at manufacturing-scale. It should be noted that, while consistent k_La conditions were required to probe other factors independently, additional DOE studies ensured an understanding of the relationship between k_La and other reaction parameters.

2.3 Enzyme development

With the aim of developing the "oxidation 2nd" sequence, we focused on the protein engineering and process goals outlined in Scheme 2. Gaining a deep understanding of each process parameter was critical for delivering a robust, scalable process and limiting the formation of byproducts (**2**, **5** and **6**) generated through non-productive enzymatic pathways (Scheme 2).

Scheme 2. Oxidation process development goals and the main byproducts generated *via* enzymatic pathways.

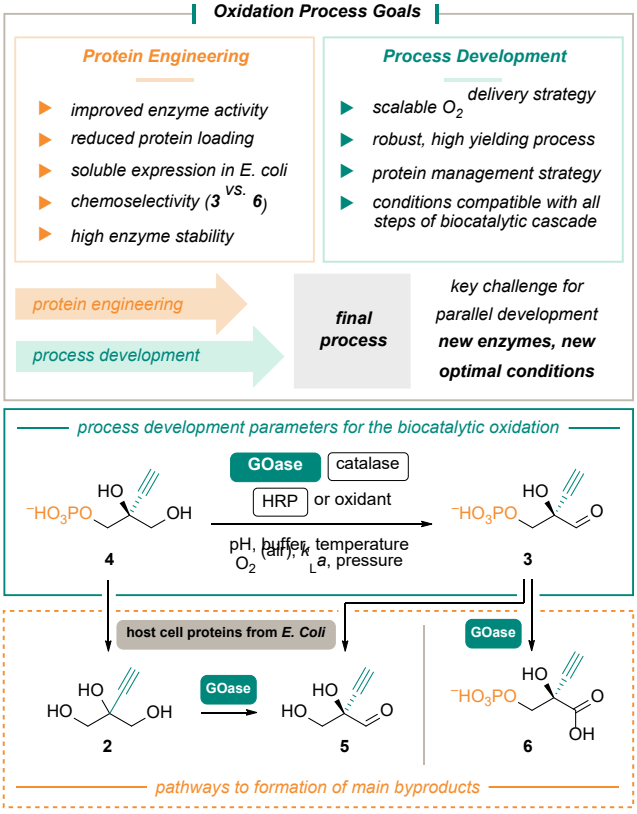

The entire islatravir biocatalytic cascade requires nine different enzymes. Seven of the enzymes were engineered variants, recombinantly expressed in *E. coli* and used as cell-free lysate powders. Consequently, reduction of the total protein content in the aqueous reaction stream was a critical factor for ensuring development of a robust process capable of delivering high-quality API.[34–37] Decreasing the overall enzyme loading was required to enable an efficient final API filtration after the aldol-glycosylation step.[34,38] Reduced protein levels also minimizes side reactions catalyzed by host cell proteins, namely phosphate hydrolysis by endogenous *E. coli* phosphatases (Scheme 2).[30] With >20 wt% $GOase_{Rd13BB}$ loading required, the highest of all nine enzymes, further evolution was needed to improve its catalytic efficiency.

2.3.1 Galactose oxidase: directed evolution, protein expression, and optimization of the active site maturation

Galactose oxidase (GOase, E.C. 1.1.3.9), the key biocatalyst used in our oxidation process, is a mononuclear copper enzyme that catalyzes a two-electron redox reaction involving an alcohol and molecular oxygen to yield an aldehyde and hydrogen peroxide as the byproduct (Figure 1A and Scheme S 1).[39] In addition to copper, the active site of GOase enzymes possess a unique, post-translationally formed Y272-C228 thioether cross-link. The covalently modified tyrosine is required for catalytic activity, functioning as a redox cofactor through transient formation of a free radical.[39] During the catalytic cycle, GOase transitions between the fully oxidized Cu(II)-Y$^{\bullet}$ state (GOase^{ox}) and the fully reduced Cu(I)-YC state (GOase^{red}). However, GOase can also exist in a semi-reduced state (GOase^{semi}), which is considered catalytically inactive (Figure 1A).[39–42] As a result, an auxiliary redox enzyme (typically peroxidase) is required to generate and maintain the active oxidation state of GOase by serving as a single-electron oxidant for GOase^{semi}.[39] Lastly, for preparative applications, GOase-mediated reactions require a catalase as a second auxiliary redox enzyme to decompose the hydrogen peroxide byproduct. Removal of hydrogen peroxide is important for both preventing enzyme deactivation and avoiding the potential safety concerns associated with disposal of peroxide-containing waste streams.

Based on initial screening data (Figure S 44) variant GOase$_{Rd13BB}$ became the new evolutionary backbone for protein engineering efforts.[1,43] Directed evolution focused on a combination of enzyme activity, thermal stability, and chemoselectivity to reduce overoxidation to acid **6** (Figure 1B, See Supporting information, Section 3 Directed evolution). With the PanK-catalyzed phosphorylation setting the chirality at the C2 stereocenter (Scheme 1), we could now accelerate evolutionary screening using achiral chromatographic assays to identify more active GOase variants. We intermittently checked the enantiopurity of aldehyde **3** obtained using the leading evolutionary oxidase variants and found that it remained constant throughout the rounds of evolution (>99% *ee*), which in combination with high yields (>90%) was indicative of high enantiospecificity in the preceding PanK-catalyzed phosporylation.[30] In parallel to activity improvements, we evaluated enzyme stability and soluble, heterologous expression in *E. coli* to ensure robust protein expression at large scale. As the oxidase activity increased, chemoselectivity towards oxidation of alcohol **4** to aldehyde **3** *vs.* overoxidation of aldehyde **3** to acid **6** became a key focus (Figure 1B, Figure S 48).

In the first round of evolution, we identified two new variants with two-fold increased activity that contained single mutations E195R (GOase$_{Rd13.010}$) and Q326R (GOase$_{Rd13.001}$ = GOase$_{Rd14BB}$) at the entrance to the active site. GOase$_{Rd13.010}$ was selected for the first multi-kilogram scale demonstration (see section 2.3.5), while we continued directed evolution in parallel. Three subsequent protein engineering rounds provided GOase$_{Rd17BB}$ with a total of five active mutations, E195R, Q326R, Q406E, L436N and G461A, and four silent DNA mutations (synonymous DNA codons) and this variant displayed an overall five-fold improvement in activity (Figure 1C/D, see Supporting Information, Directed evolution section, Figure S 46-Figure S 49). Copper-bound GOase$_{Rd17BB}$ maintained high activity even when exposed to temperatures up to 45 ˚C (Figure 1B and Figure S 47, 30 °C for the copper-free pro-peptide), which was critical for large-scale fermentation and process robustness. Protein engineering efforts, along with the change in the order of steps, improved the phosphorylation-oxidation sequence and delivered (*R*)-**3** in >85% assay yield and >99% *ee* (Figure S 48) with minimal formation of the overoxidation byproduct **6** (<5%).

To minimize the copper and oxidase toxicity to the *E. coli* host, the enzyme is expressed in the absence of copper to produce a metal-free pro-GOase protein.[18,44] Post-fermentation cell disruption and downstream processing yields copper-free, crude lysate powders that can be stored, handled, and shipped in a manner analogous to other raw materials. At shake-flask scale, the copper-free protein expression strategy led to the formation of significant amounts of insoluble protein (up to 50%, Figure S 49). However, enzyme powders produced in a fed-batch, fit-for-purpose fermentation displayed two-fold improvement in activity (Figure S 50). Further optimization of the fermentation and downstream processing at the vendor facility led to a two-fold increase in the activity of the GOase$_{Rd17BB}$ powders. These advances, in conjunction with protein engineering, proved critical for achieving our goal of reducing overall protein burden as well as minimizing host cell proteins in the cascade reaction streams.

To form the catalytically active oxidase, the pro-GOase peptide must undergo multiple post-translational modifications: copper incorporation at the active site, followed by formation of the covalent Y272-C228 thioether bond, and then generation of the active Cu(II)-Y$^{\bullet}$ radical species (Figure 1A, GOase^{ox}).[44–46] We investigated the conditions under which the GOase enzyme powder is combined with the copper source to ensure that the active enzyme is generated efficiently (see Section 2.4.1). Preliminary studies identified copper(II) sulfate as an appropriate copper source. Importantly, while higher copper loadings lead to increased oxidation reaction rates, we found that increasing the copper concentration had a detrimental impact on the aldol-glycosylation step (Figure S 31-Figure S 32).[34] We hypothesize that this effect is due to inhibition of the manganese(II)-dependent phosphopentomutase enzyme, highlighting the challenge of developing a unified reaction system for nine different enzymes.[34] Spectroscopic (Figure S 2) and preparative studies (Figure S 5-Figure S 8) confirmed that copper complexation/thioether bond formation does not require molecular oxygen when copper(II) salts are employed (Figure S 5), consistent with prior reports.[45] UV-Vis data indicated that the addition of copper(II) to the pro-GOase$_{Rd17BB}$ peptide under aerobic aqueous conditions yielded predominantly the semi-reduced, catalytically inactive GOase^{semi}, highlighting the importance of GOase activation (Supporting Information, section 1.4.3)[39,45]

2.3.2 Auxiliary enzymes: peroxidase and catalase

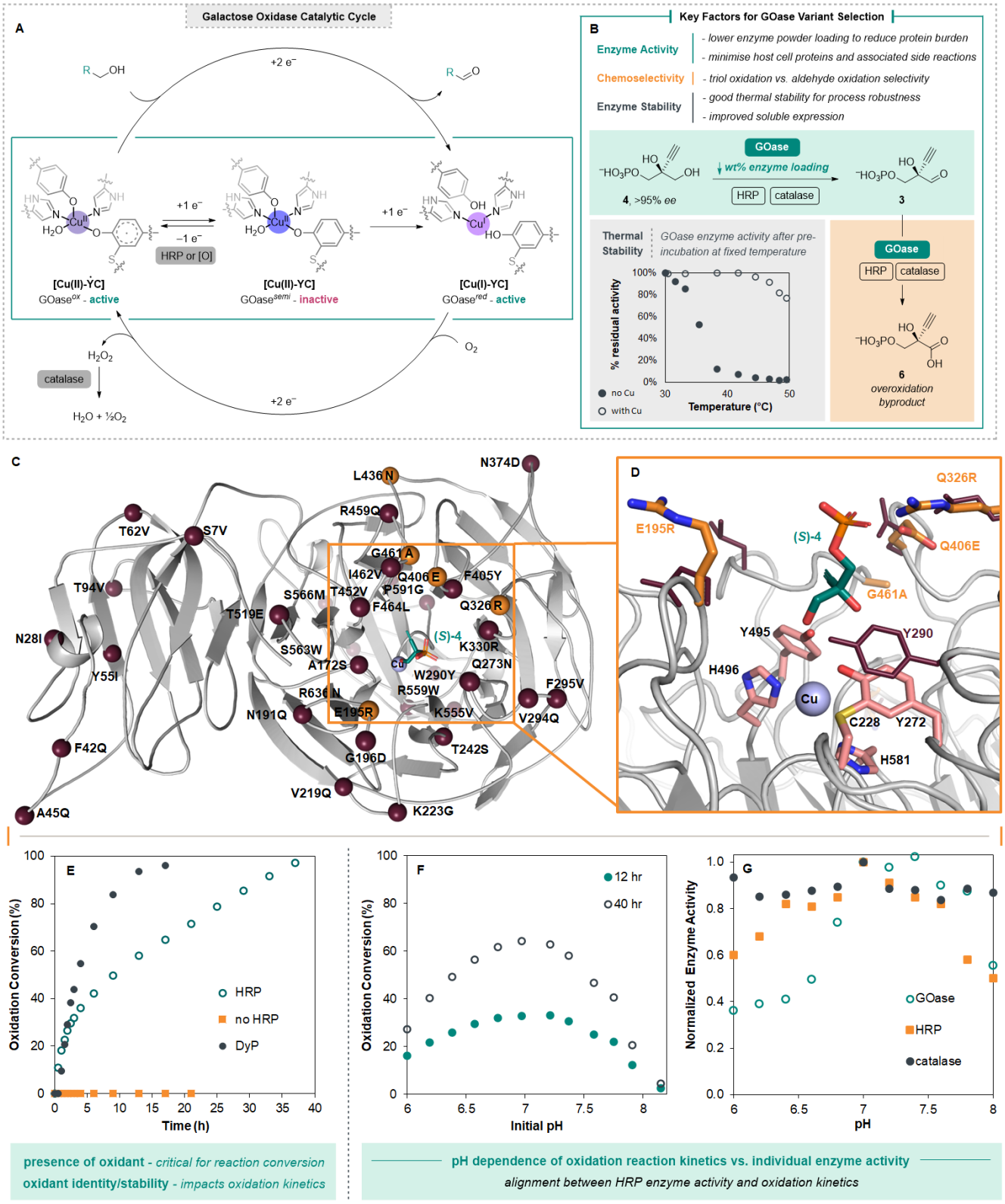

Figure 1A: Simplified catalytic cycle of galactose oxidase, adapted from ref[39,45]. **B**: Factors used to select GOase variants during enzyme evolution (see SI for details). **C:** Computational model of evolved GOase$_{Rd17BB}$ structure and active site, highlighting the mutations introduced during the evolution programs towards 2-ethynylglycerol **2** (●, rounds 1-12) and this work (●, rounds 13-16) based on the crystal structure (PDB ID: 8TX6). **D**: Active site showing copper atom (●), key copper-binding residues (●: Y465, H496, H581 and Y272 forming thioether bridge with C228), (*S*)-2-ethynylglycerol 1-phosphate substrate **4** (●). **E**: Evaluation of different oxidants, oxidation reaction profile with no HRP (■), HRP (○) and DyP$_{Rd3BB}$ (●). **F**: Comparison of oxidation kinetics for reactions with different starting pHs. Reaction conversion at 12 hours (●) and 40 hours (○). **G:** Enzyme activity (as determined by enzyme activity assay) at different pHs; GOase (○), HRP (■) and catalase (●).

In addition to formation of GOase^{semi} upon initial copper incorporation, prior literature studies indicate that this inactive state can be generated during the reaction *via* an off-cycle 1e$^-$ reductive deactivation pathway from GOase^{ox}. Consequently, a single-electron oxidant is required to both activate the initial GOase^{semi} species formed and then continue to rebound GOase^{semi} to GOase^{ox} during the reaction. Horseradish peroxidase (HRP) and a wide range of single-electron oxidants can serve as activators for GOase.[39,47] The mechanism by which electron transfer between HRP and galactose oxidase occurs is not well understood. Interestingly, in a structurally and functionally-related family of glyoxal oxidases, the enzymes are activated by Mn(III) glyoxylate, which itself is generated by one-electron oxidation of Mn(II) by a lignin peroxidase.[48,49] However, to date no mediator has been associated with GOase activation by HRP. Recent work by Forget *et al*.[50] and Kosman *et al*.,[51] as well as studies on protein modification,[52,53] suggest that HRP can directly oxidize solvent-exposed tyrosines or tryptophans, potentially leading to the formation of the Cu(II)-Y$^{\bullet}$ active site radical *via* electron hopping from the protein surface.[54,55]

During early process development studies, we demonstrated that a variety of single electron oxidants, including Mn(III) salts[40] and electrochemically regenerated mediators,[41] can serve as activators for the GOase$_{Rd10BB}$ catalyzed oxidation of 2-ethynylglycerol (**2**). To choose the optimal activator for the manufacturing scale oxidation of (*S*)-2-ethynylglycerol 1-phosphate (**4**), we rescreened a focused panel of peroxidases and single-electron oxidants with GOase$_{Rd13BB}$ (see Supporting information section 1.4.3). Horseradish peroxidase and Mn(III) salts gave the highest conversions to aldehyde **3**. Mn(III) acetate and HRP, both commercially available at scale, were further investigated with GOase$_{Rd17BB}$ (Figure S 10). While we observed comparable reaction rates with both oxidants when using GOase enzyme powders in solution, Mn(III) acetate gave variable reaction performance in conjunction with immobilized oxidase enzymes (data not shown), which we attributed to the poor solubility of Mn(III) salts in the aqueous buffer. The use of Mn(III) acetate also led to challenges with subsequent filtrations in the cascade process, and this combination of factors ultimately drove our decision to select horseradish peroxidase for large scale process development (See SI section 1.4.3).

Next, we evaluated the impact of peroxidase stoichiometry on the oxidation reaction (Supporting information Section 1.4.3.5). In the absence of HRP, minimal conversion of **4** to **3** occurred when GOase$_{Rd17BB}$ was employed (Scheme 1E). While HRP loadings ranging from 0.06-3 wt% gave comparable initial reaction kinetics, higher peroxidase concentration reduced the time required to meet the target reaction conversion (>90%). During process characterization, the cost of HRP was balanced with the relatively minor reduction in reaction time afforded by higher HRP loadings and we selected a target enzyme loading of 0.3 wt% HRP.

Employing reaction monitoring tools, we investigated the oxidation reaction profile and observed apparent two-phase kinetics for the oxidation reaction; a fast initial, linear burst, followed by a second, linear phase (Figure 1E and Figure S 13). Based on enzyme activity studies (see section 2.3.3 and 2.4.2), we attributed the slower kinetics in the latter phase of the reaction to decreasing activity and/or inhibition of HRP and resultant slower rebound of the inactive GOase^{semi} to the active GOase^{ox}. Two subsequent experiments supported this hypothesis. Firstly, sequential dosing of HRP throughout the reaction (Figure S14, 3 portions at 0, 3 and 17 h) led to shorter reaction times *vs.* dosing the same quantity of HRP as a single charge at the start of the reaction. Secondly, heme-dependent recombinant DyP$_{Rd3BB}$ peroxidase from *Anabaena sp*.[56] gave single phase kinetics and shorter reaction times were observed (Figure 1E and Figure S 13). While the use of DyP peroxidase is not currently viable for large-scale manufacturing, this study highlights that the choice of peroxidase/oxidant can profoundly impact oxidation kinetics and underlines the need for further understanding of the mechanism of GOase activation.[48–51,57]

Finally, identification of a robust, stable catalase to decompose the hydrogen peroxide side product was required (Figure 1A). We evaluated bovine and microbial catalases (Figure S 14). With many commercial enzymes displaying comparable oxidation reaction kinetics, we chose catalase from *Corynebacterium glutamicum*. This bacterial enzyme displayed excellent stability in solution (data not shown), high activity across a wide range of enzyme loadings (0.06 to 1.2 wt%, Figure S13) and avoided the use of an animal-derived biocatalyst in the process.

2.3.3 pH dependence: reaction kinetics and individual enzyme activity

With the final manufacturing enzyme variants selected, we reevaluated the impact of pH on the overall reaction kinetics and the activity of each of the three oxidation enzymes (see Supporting Information, Figure S 15-Figure S 16). Full conversion to product occurred across a wide pH range (pH 6.4-7.8) and the pH of the oxidation stream decreases slightly as the reaction approaches full conversion when the over-oxidation acid byproduct **6** begins to form. The optimal pH for the oxidation reaction is centered around pH 7 (Figure 1F) and mirrors the pH-activity profile of HRP (Figure 1G). In contrast, the pH optimum of GOase$_{Rd17BB}$ appears slightly shifted (pH 7.0-7.8), and catalase exhibits comparable activity across the entire pH range evaluated (pH 6.0-8.0). These observations further support the hypothesis that oxidation reaction kinetics are correlated with peroxidase activity and maintenance of the active GOase enzyme over the course of the reaction.

2.3.4 Immobilized enzyme process development

With parallel protein engineering and process development efforts ongoing, we investigated alternative approaches for minimizing protein burden across the cascade[29] to enable robust isolation and crystallization of the API.[34,58] Enzyme immobilization presents an attractive strategy for protein removal. We focused on a His$_6$-tag affinity-based immobilization for both the GOase and PanK enzymes (Figure 3A).[1,26,59] Compared to other approaches, it offers several advantages: (*i*) selective binding of recombinant His$_6$-tag

enzymes on resin; (*ii*) removal of *E. coli* host cell proteins during resin washes to help minimize side reactions, providing stable product streams in the absence of isolations during the cascade,[1] (*iii*) generality and fast development time as this immobilization platform can be applied to many different enzymes,[60] and (*iv*) compatibility with aqueous reaction conditions. For GOase specifically, immobilization in the presence of copper(II) salts enables active site maturation (see Section 2.3.1, Figure 3A) and excess unbound copper can be removed during the post-immobilization washes. Critically, this avoids any detrimental impact of excess copper on the subsequent aldol-glycosylation step (see also SI, Section 1.7.2).[34] Additionally, separation of the immobilized GOase enzyme from the reaction stream can help prevent the formation of byproducts due to over-oxidation during storage or subsequent steps.

Development of a robust metal affinity-based immobilization strategy requires consideration of the resin bead material and physical properties, the coordinating metal and binding ligand, and the immobilization conditions.[61] We established a protocol to immobilize His_6-tagged $GOase_{Rd13.010}$ onto Bio-Rad Nuvia IMAC resin, a bioprocess-grade, vinylacrylamide resin functionalized with nitrilotriacetic acid (NTA) ligands chelated with nickel (Figure 3A). In a practical sense, immobilization involved rehydration of the enzyme powders in a high salt binding buffer containing 15 mM imidazole (to prevent non-specific binding of host-cell proteins) and copper(II) sulfate (to generate Cu-charged GOase), followed by exposure to the resin of interest. After immobilization was complete, the resin-bound enzyme was washed repeatedly with binding buffer followed by reaction buffer (50 mM Bis-Tris, pH 7-8) to remove unbound host cell proteins, excess copper, and immobilization reagents and salts. The resultant immobilized copper-charged enzyme was directly transferred to the reaction vessel as a slurry in the reaction buffer. Importantly, upon completion of the oxidation step, simple filtration enabled facile removal of the immobilized biocatalysts and provided a robust end of reaction protocol, preventing further over-oxidation of aldehyde **3**. Using the outlined immobilization strategy, oxidation of alcohol **4** delivered aldehyde **3** in >80% yield in lab-scale experiments. Notably, these experiments represented the first demonstration of a fully continuous aqueous cascade process from triol **2** to deliver high-quality API, eliminating the requirement for any isolations or purity upgrades.[29]

In addition to bioprocess-grade IMAC resin (Bio-Rad Nuvia IMAC), we evaluated process-scale resins such as methacrylate polymer-based Purolite Chromalite MIDA and Resindion Relizyme IDA403/S resins, containing iminodiacetic acid (IDA) chelating ligands that coordinate nickel (Figure 3B). While the IDA divalent ligand-based resins possess a higher capacity for enzyme binding *vs.* the trivalent NTA ligand resin,[62] GOase immobilized on IDA-resins displayed decreased performance in the reaction, necessitating a two-fold increase in enzyme loading to achieve complete conversion. In addition, the polydispersity of these resins caused variable filtration rates and we chose to proceed with use of the Bio-Rad Nuvia IMAC resin for large scale demonstration of the immobilized process.

2.3.5 Immobilized enzyme pilot plant-scale demonstrations

The first demonstration of the immobilized process at pilot plant scale was achieved using $GOase_{Rd13.010}$ at 12 wt% enzyme loading immobilized on the Bio-Rad Nuvia IMAC resin at 50 g enzyme per 1 L resin (see Figure 4**,** PPB1). Immobilized kinase and oxidase enzymes were both freshly prepared in the pilot plant and then slurry charged to the phosphorylation and oxidation batches, respectively. Removal of the immobilized kinase enzyme from the phosphorylation stream before the oxidation reaction was not required. Both immobilized enzymes were filtered off before the aldol-glycosylation step as both 2-fluoroadenine and islatravir are poorly water-soluble, rendering the final portion of the cascade a slurry-to-slurry reaction. Importantly, removal of the immobilized oxidase enzyme prevented any over-oxidation of aldehyde product **3** to acid **6** from occurring during stream storage. The oxidation step reached the target conversion (>90%) within 21 h to give aldehyde **3** in 83% yield (Figure 4). Critically, the aldehyde stream obtained using immobilized phosphorylation and oxidation enzymes was successfully carried through the aldol-glycosylation step and final filtration to deliver API meeting all specifications.

While deployment of immobilization ensured successful isolation of high-quality API, we recognized several challenges regarding its transfer to manufacturing scale, namely: (*i*) the large volume and high cost of the resin, (*ii*) the need for slurry transfers on plant scale and (*iii*) the requirement for additional operations, vessels, and equipment trains to execute washes and filtrations. We sought to address these issues prior to further plant scale demonstrations. We achieved a >three-fold reduction in the required resin volume (Figure S 26) by combining improvements in GOase activity ($GOase_{Rd17BB}$ *vs.* $GOase_{Rd13.010}$, Figure S 48-Figure S 50) with optimization of the enzyme: resin ratio (from 50 g enzyme powder per L resin to 80 g/L**,** Figure S 26-Figure S 27). These advances simplified operations and decreased the cost of goods.

To address the outstanding operational issues, we envisaged lyophilization of the immobilized oxidase and kinase enzymes.[30] Using this approach, enzyme immobilization could be decoupled from the API manufacturing campaign and the immobilized lyophilized enzyme could be prepared at an external facility, alleviating the need for additional equipment (*i.e.*, immobilization vessels and filters) and decreasing processing times. Proof-of-concept was achieved for the use of immobilized, lyophilized GOase enzymes and, as anticipated, these enzymes could be conveniently handled and charged as a typical solid reagent. Small-scale development studies showed that, while the immobilized lyophilized enzyme (2.15 wt% water) displayed slightly reduced activity *vs.* freshly immobilized enzyme, the lyophilized immobilized enzymes retained their activity on storage for several weeks (Figure 3C). Subsequent work established that control of the water content of the lyophilized resin (<2 wt%) and cold storage (-20 °C) are critical for retaining maximal catalytic activity. Our immobilization-lyophilization approach was demonstrated in a subsequent pilot plant campaign (Figure 4, PPB4). This multi-kilo scale batch utilized immobilized lyophilized enzymes in both the

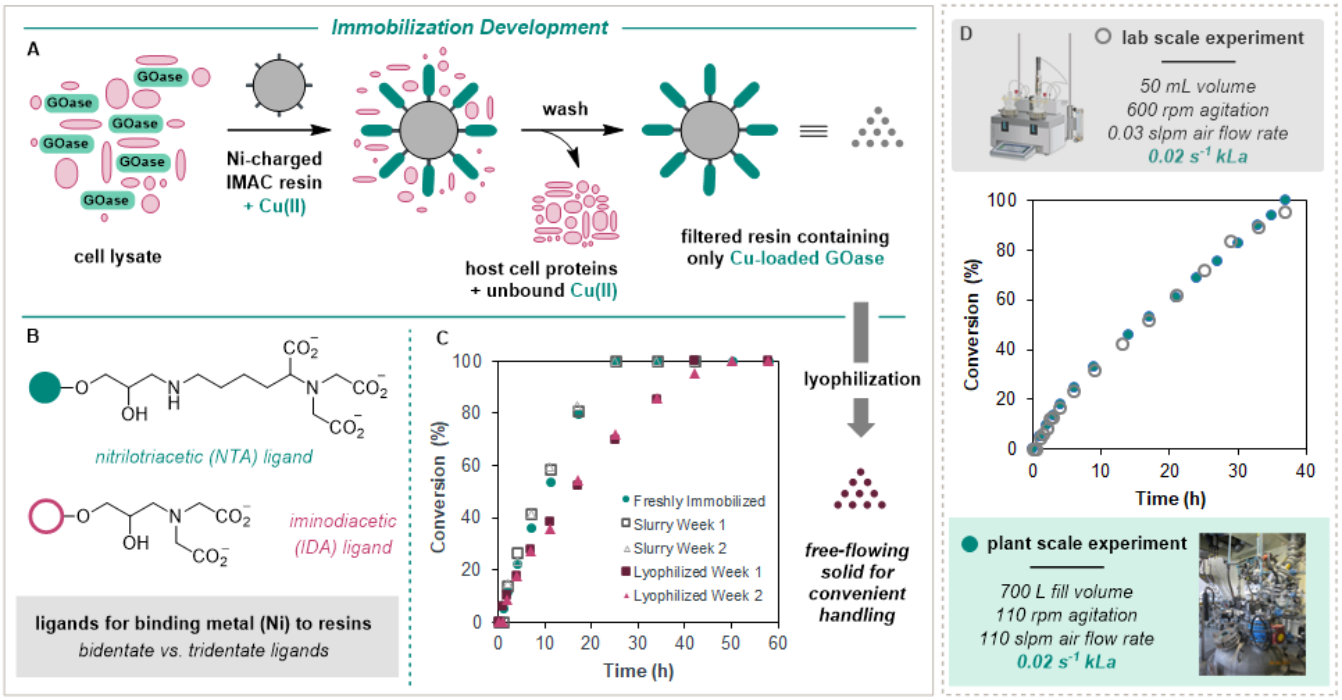

Figure 3A: Schematic illustrating the immobilization procedure. **B**: Nitriloacetic acid (NTA) ligand on Bio-Rad Nuvia IMAC resin and iminodiacetic acid (IDA) ligand on the Purolite Chromalite MIDA and Resindion Relizyme resins. **C**: Stability of immobilized lyophilized $GOase_{Rd17BB}$ on Bio-Rad Nuvia IMAC resin. Reaction profiles obtained with enzymes freshly immobilized (●), stored 1-2 week as a slurry (□△) or lyophilized resin (■▲). **D**: Pilot plant demonstration of the immobilized oxidation process (●, PPB4) *vs.* lab-scale front-run experiment (○).

	PPB1	PPB4	PPB5
Oxidation Scale	26.6 kg	20.7 kg	14.4 kg
Oxidase	12 wt% immobilized $GOase_{Rd13.010}$	6.5 wt% immobilized lyophilized $GOase_{Rd17BB}$	3.6 wt% $GOase_{Rd17BB}$ lyophilized powder
Fermentation	fit-for-purpose	fit-for-purpose	optimized
Resin Quantity	576 mL resin per 1 kg triol **8**	165 mL resin per 1 kg triol **8**	no resin
Peroxidase	0.6 wt% PEO-301	0.6 wt% PEO-301	0.3 wt% POD II
Catalase	0.3 wt% Bovine catalase	0.3 wt% *corynebacterium glutamicum* catalase	0.3 wt% *corynebacterium glutamicum* catalase
Copper (II) sulfate	in immobilization	in immobilization	50 μM conc
Temperature	17 °C	17 °C	5 °C
k_La	0.04 s^{-1} k_La	0.02 s^{-1} k_La	0.007 s^{-1} k_La
Pressure	1 atm	1 atm	2.9 atm
Reaction time	21 hours	39 hours	19.5 hours
Yield from triol 2	83% yield	87% yield	90% yield

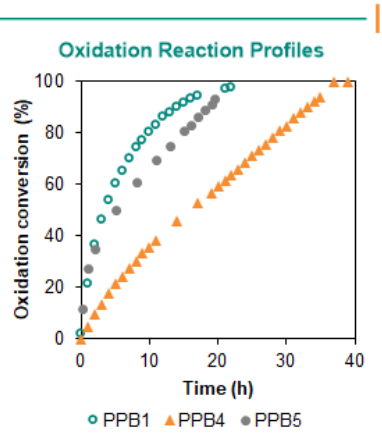

Development Highlights

- *3-fold reduction in oxidase loading*
- *eliminated immobilization process*
- *demonstrated elevated pressure enzymatic aerobic oxidation*
- *success across relevant k_La range*

Figure 4: Comparison of process conditions and reaction profiles for the pilot plant batches, PPB1 (○), PPB4 (▲) and PPB5 (●).

phosphorylation (PanK) and oxidation (GOase) steps. For the oxidation, two-fold reduced loading of oxidase enzyme (6.5 wt% $GOase_{Rd17BB}$ *vs.* 12 wt% $GOase_{Rd13.010}$) and >three-fold reduced resin volume (576 *vs.* 165 mL resin/1kg of triol **4**) were required, delivering aldehyde **3** in 87% yield.

Importantly, the plant processing time was reduced compared to PPB1.

Beyond successful demonstration of the immobilized process, conducting these two pilot plant batches enabled evaluation of the oxygen mass transfer control strategy and reproducibility of the reaction at scale. While the first pilot plant batch was conducted at a k_La of 0.04 s^{-1}, the second pilot plant batch was conducted at a k_La of 0.02 s^{-1}, closer to the value we expected to achieve in manufacturing scale vessels. Both pilot plant batches reached the target conversion within 40 h and, most importantly, the reaction rate in the plant closely aligned with the reaction profile observed in the lab. As shown in Figure 3D, the kilo-scale batch showed comparable reaction kinetics to gram-scale reactions in the lab, providing further confidence in our k_La characterization methodology and oxygen mass transfer control strategy.

2.4 Non-immobilized enzyme process considerations

Enzyme immobilization was key to the success of the initial large-scale demonstrations of the islatravir biocatalytic manufacturing process. Despite the advances made during development of the immobilized process, the resin remained a major cost contributor to the manufacturing process and immobilization/lyophilization of the enzymes at an external manufacturing site increased supply chain complexity. Additionally, further understanding of the lyophilization process parameters and factors impacting immobilized lyophilized enzyme stability were required (*e.g.*, water content).

During immobilized enzyme process development, directed evolution continued for all the enzymes in the cascade and this resulted in >two-fold reduction in the overall enzyme loading (from 40 wt% to 15 wt%, PPB1 *vs.* PPB5, Table S 1).[29] Consequently, we re-evaluated the possibility of using non-immobilized, lyophilized enzyme powders in both the phosphorylation and oxidation steps. Decreased enzyme loading and extensive API isolation studies rendered the final islatravir filtration and crystallization feasible for an entirely immobilization-free enzyme cascade.[34,58] We were able to minimize the phosphatase activity of the crude, lyophilized enzyme powders through protein expression and fermentation optimization studies.[30] Using these enzyme powders, the aqueous triol **4** and aldehyde **3** streams were stable for at least two weeks with minimal phosphate cleavage observed (<5% assay yield loss). While these advances addressed several major issues, removal of the immobilization step introduced new challenges for the oxidation reaction; (*i*) the requirement for an alternative end-of-reaction control strategy to prevent over-oxidation of **3**, and (*ii*) the presence of unbound copper in the reaction stream and its impact on the aldol-glycosylation cascade. Herein, we describe the development and large-scale demonstration of a non-immobilized enzyme oxidation process.

2.4.1 Non-immobilized enzyme process development

The development of a non-immobilized enzyme process required a deep understanding of the pro-GOase peptide maturation to ensure that GOase enzyme activity was maximized while the impact of unbound copper on the aldol-glycosylation enzymes was minimized (Figure S 31). For the immobilized process, the risk of unbound Cu was mitigated by removal in post-immobilization washes (Figure 3A). Initial studies showed improved and more reproducible non-immobilized enzyme reaction performance when the GOase and Cu(II) sulfate were premixed in water prior to charging to the oxidation stream *vs.* charging GOase and Cu(II) salts separately to the batch. We hypothesized that complexation of Cu within the GOase active site occurs more efficiently in the absence of other coordinating species in the aqueous reaction stream (*e.g.,* other proteins, Bis-Tris buffer, salts). In addition, we evaluated the possibility of premixing and charging all three oxidation reaction enzymes (GOase, HRP and catalase) together as a solution in water with Cu(II) sulfate (Figure S 8). Premixing catalase and Cu(II) in solution was detrimental to the oxidation performance and, consequently, HRP and catalase were charged separately as solids to the reaction vessel. Detailed studies were conducted on the premixing step, probing the impact of enzyme concentration, time, temperature, oxygen/inert atmosphere, and Cu loading on the oxidation reaction performance. While enzyme concentration, time, and temperature had minimal impact over a wide operating range, Cu loading significantly affected the oxidation reaction rate (Figure 5, Figure S 5-Figure S 7).[45]

Next, we sought to understand the relative impact of copper concentration on both the oxidation and aldol-glycosylation reactions (See SI section 1.2.2 and 1.4.1). As shown in Figure 5, use of low Cu loadings (20 μM concentration relative to overall reaction volume) resulted in incomplete conversion in the oxidation reaction. Increasing the Cu loading (50 μM) led to an increase in the oxidation rate of reaction, ensuring that the target oxidation conversion could be reached, and the stream was successfully taken forward through the aldol-glycosylation reaction to deliver quality API. At higher Cu loadings (100 μM) the oxidation reaction kinetics continued to improve but, at this stage, the elevated unbound Cu levels began to have a detrimental impact on the aldol-glycosylation reaction (23 h *vs.* 10 h reaction time). Addition of EDTA after the oxidation step to sequester excess Cu gave modest improvements in the aldol-glycosylation reaction rate but this approach could not be translated into a robust control strategy (Figure S 31). Consequently, detailed DOE studies allowed us to determine a Cu(II) sulfate loading range that balanced the impact of Cu on both parts of the biocatalytic sequence, ensuring the success of both steps within an appropriate time frame.

Finally, we developed a reliable control strategy for preventing GOase-mediated overoxidation of aldehyde product **3** to acid byproduct **6** upon reaction completion and stream storage. In contrast to the immobilized process, removal of the oxidase enzyme was no longer possible. Instead, upon reaching the target oxidation conversion, we removed oxygen by sweeping the vessel headspace with an inert gas. This end-of-reaction control strategy was robust and simple to implement in the plant.

2.4.2 Oxygen mass transfer considerations at manufacturing scale

To ensure process portability, we sought to develop a robust oxidation process that could be successfully implemented in reactors where the maximum achievable k_La value is lower than 0.02 s^{-1}. While we had successfully demonstrated reproducibility across scales, lab-scale experiments showed that oxidations run at lower k_La (<0.015 s^{-1}) carried a risk of incomplete conversion at the extremes of our operating ranges. Reconfiguring reactors in manufacturing plants to achieve higher k_La requires significant capital investment and therefore future studies focused on improving oxygen mass transfer by changing the thermodynamic driving force (*i.e.,* increasing the maximum concentration of oxygen in solution, see Section 2.2).[32] In practical terms, three different parameters could be leveraged to alter the thermodynamics of oxygen mass transfer: *i*) oxygen concentration in the gas feed, *ii*) pressure, and *iii*) temperature.

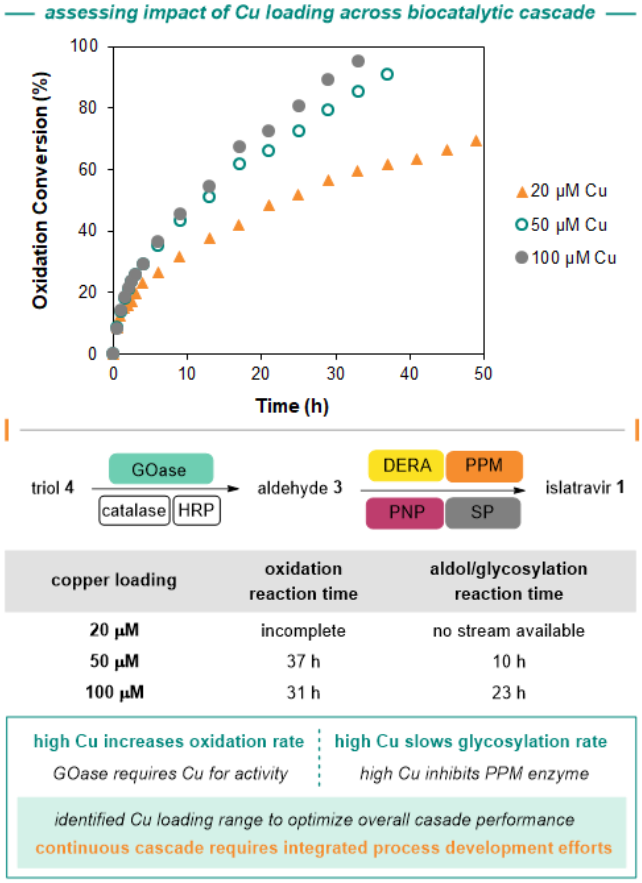

copper loading	oxidation reaction time	aldol/glycosylation reaction time
20 µM	incomplete	no stream available
50 µM	37 h	10 h
100 µM	31 h	23 h

Figure 5: Impact of copper(II) sulfate charge on oxidation reaction kinetics: 20 µM (▲), 50 µM (○) and 100 µM (●), and the subsequent aldol-glycosylation step.

Firstly, we considered the use of gases with a higher oxygen concentration than air (21% O_2). Indeed, increasing the gas oxygen concentration to 40% or 100% resulted in a faster reaction rate (Figure S 25). While these results supported our hypothesis, the supply and safety concerns associated with using enriched or pure oxygen gases in manufacturing facilities drove efforts to identify an alternative solution.

Next, we evaluated the performance of the oxidation reaction at elevated pressure. Increasing the pressure from 1 atm to 3.7 atm decreased the reaction time from >60 h to 30 h under low k_La conditions (0.013 s^{-1}, Figure 6). The considerable rate enhancement observed at <4 atm pressure renders this an attractive option for plant-scale synthesis, as the process could be readily transferred to a standard manufacturing vessel with minimal capital investment (*i.e.*, without requiring specialized high-pressure vessels).

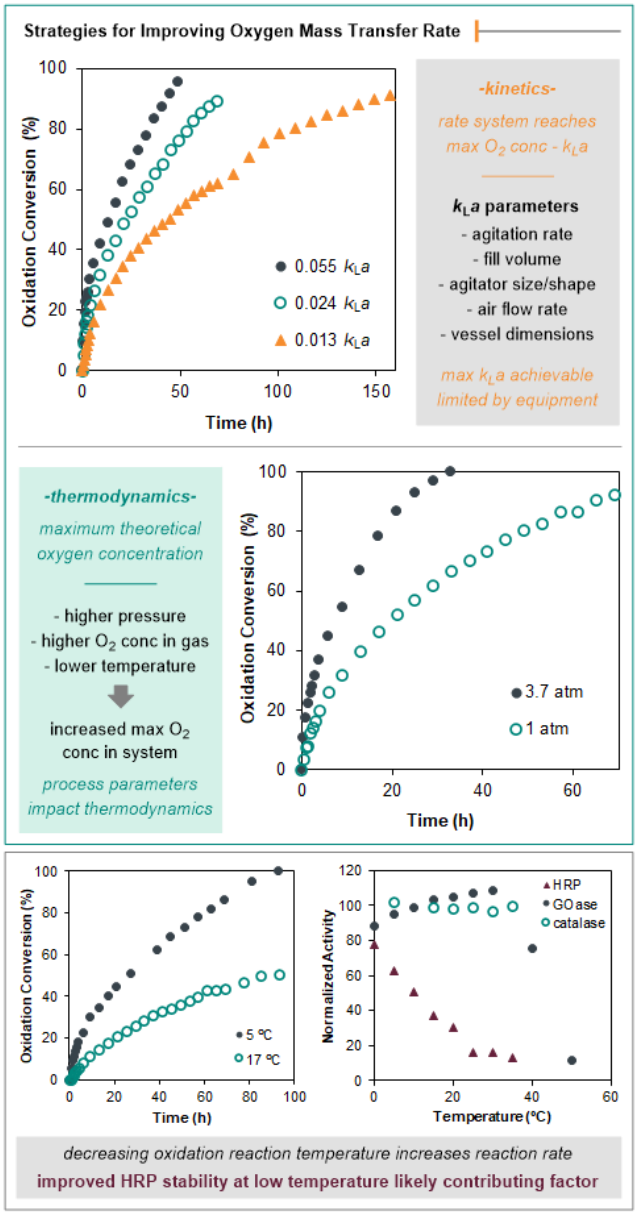

Figure 6: Optimization of factors impacting oxygen mass transfer rate. Top: Impact of k_La on oxidation reaction kinetics, 0.055 s^{-1} (●), 0.024 s^{-1} (○) and 0.013 s^{-1} (▲). Middle: Impact of elevated pressure on oxidation reaction kinetics (k_La: 0.013 s^{-1}), 3.7 atm (●) and 1 atm (○). Bottom left: Impact of temperature on oxidation reaction kinetics (k_La: 0.07-0.08 s^{-1}), 5 °C (●) and 17 °C (○). Bottom right: Enzyme activity after preincubation at different temperatures, HRP (▲), GOase (●) and catalase (○).

Finally, we investigated the impact of reaction temperature on the process. While oxygen solubility increases at lower temperatures, k_La typically decreases and the impact of temperature on the activity of the oxidation enzymes was unknown. In fact, we observed faster reaction kinetics at 5 °C and reactions run under k_La conditions as low at 0.007 s^{-1} reached full conversion (Figure 6). The substantial improvement in reaction performance led us to investigate the thermal stability of each oxidation enzyme. The activity of each enzyme was evaluated after pre-incubation of the enzyme in buffered solution at different temperatures (Figure 6). While the activity of the GOase and catalase enzymes was maintained from 0-35 °C, a large reduction in HRP activity was observed when the enzyme was held in solution at temperatures above 0-5 °C. These stability experiments indicate that HRP activity contributes to the improved reaction performance at low temperature, which aligns with our previous studies associating HRP activity with overall reaction performance (see section 2.3.2).

2.4.3 Non-immobilized enzyme pilot plant-scale demonstration

By combining the outlined strategies for improving oxygen mass transfer rate with our expanded understanding of GOase maturation and copper loading effects, we were able to demonstrate the non-immobilized GOase process at pilot plant scale for the first time (Figure 4, PPB5). Here, the pro-GOase peptide was combined with the Cu(II) sulfate and this solution was charged directly to the reaction vessel, reducing the processing time, cost, and waste associated with the immobilization process. We successfully conducted the oxidation process under low k_La conditions (0.007 s^{-1}) by employing elevated pressure (2.9 atm) and low temperature (5 °C) process conditions. The target oxidation conversion was achieved in 19.5 h, providing aldehyde **3** in 90% yield. Finally, the aqueous stream of **3** containing non-immobilized GOase and PanK enzymes was successfully carried forward into the aldol-glycosylation cascade and final isolation to deliver high purity islatravir product **1**.[34]

3. Conclusions

To successfully translate enzymatic reactions to scalable, industrial processes, it is necessary to combine efforts in biocatalyst and reaction engineering.[24] During our work developing the enzymatic aerobic oxidation within the islatravir biocatalytic cascade, we improved the activity and selectivity of galactose oxidase variants using protein engineering and enzyme expression optimization. Mechanistic understanding of enzyme maturation and catalysis was critical for advancing reaction development. Parallel process development efforts utilized enzyme immobilization as a critical interim strategy for addressing high protein burden, enabling the first kilo-scale plant demonstrations. We addressed challenges related to efficient delivery of oxygen at manufacturing scale through rigorous characterization of the volumetric mass transfer coefficient (k_La) across scales and modulation of process parameters that impact the thermodynamics of oxygen mass transfer.[31,32] By utilizing elevated pressure and low temperature, we maximized enzyme efficiency with minimal capital investment required for modifications to the manufacturing equipment.[11,63–66] Combined protein engineering and process development efforts obviated the need for enzyme immobilization, further simplifying the execution of the aerobic oxidation on industrial scale. Under optimized reaction conditions, the final engineered biocatalyst GOase$_{Rd17BB}$ selectively converts (*S*)-2-ethynylglycerol 1-phosphate (4) to aldehyde **3** in 90% yield and with a low enzyme loading of 3.6 wt%. As the toolbox of oxygen-dependent biocatalysts continues to expand,[3] our studies pave the way for the future development of enzymatic aerobic oxidations in chemical manufacturing.

4. Experimental section

4. 1 Chemicals

(S)-2-ethynylglycerol 1-phosphate (**4**) was synthesized as described previously[30] and provided as 50 mM Bis-Tris buffer solution. Nuvia IMAC resin was purchased from Bio-Rad. All other chemicals were obtained from commercial vendors. Peroxidase and catalase enzymes were purchased from Sigma (USA), Roche Custom Biotech (USA), Toyobo (JP) or Codexis (USA). All the details of enzyme evolution, expression in *E. coli* as well as reaction optimization and analytical assays are described in the **ijujki**.

4.1 Pilot-scale procedures

Pilot plant batch 1 (PPB1): Synthesis of (*R*)-2-ethynylglyceraldehyde 3-phosphate (**3**) using freshly immobilized GOase$_{Rd13.010}$

Generation of immobilized GOase$_{Rd13.010}$ resin slurry: Binding buffer (72 L, 50 mM sodium phosphate, 500 mM NaCl, 15 mM imidazole, pH 8.0) was charged to an equipped with a mechanical stirrer, followed by copper sulfate pentahydrate (40 g, 1 g per 80 g of enzyme lyo powder) in binding buffer (200 mL). GOase$_{Rd13.010}$ (3.183 kg, 12.0 wt% relative to **4,** fit-for purpose fermentation powder) was charged and the enzyme and copper (II) mixture was agitated until the enzymes were fully rehydrated in solution. A slurry of Bio-Rad Nuvia IMAC resin (127.3 L, 50 vol% in 20% EtOH) was charged to a filter dryer and the resin was filtered to remove EtOH. The resin was slurry washed with water (4 × 119.4 L, total water: 477.4 L, 7.5 resin-bed volumes) and each slurry wash was agitated for at least 15 minutes prior to filtration. The resin was then slurry washed with binding buffer (119.4 L, 1.9 bed volumes) for 15 minutes before filtration. The GOase$_{Rd13.010}$ and copper (II) solution was transferred into the filter dryer containing the washed Nuvia resin, followed by a flush with binding buffer (20 L). The enzyme and resin slurry were agitated in the filter dryer at 20-25 °C for 3 h. The binding buffer solution was filtered off. The resin wet cake was slurry-washed with fresh binding buffer solution (5 × 119.4 L, 15 min agitation each, total buffer: 597 L, 9.4 resin-bed volumes), followed by washes with reaction buffer (50 mM Bis-Tris methane buffer pH 8, 5 × 119.4 L, 15 min agitation each, total 9.4 resin bed volumes). The immobilized enzyme was then resuspended in 50 mM pH 8 Bis-Tris methane buffer (1 × 95.5 L, 1.5 bed volume) and used in the oxidation reaction.

Oxidation reaction: (*S*)-2-ethynylglycerol 1-phosphate (**4**, 137.1 mol, 350 kg of 7.6 wt% solution) in Bis-Tris methane buffer[30] was charged to a vessel equipped with a jacket, mechanical stirrer, temperature probe, dissolved oxygen sensor, pH probe and air subsurface line and the solution was adjusted to 17 °C. The pH of the reaction mixture was adjusted to pH 7.25 through the addition of 5 M KOH (10.2 kg). Bovine catalase (80 g, 0.3 wt% relative to **4**, Sigma C1345) in water (4 L) and horseradish peroxidase (160 g, 0.6 wt% relative to **4**, Toyobo PEO-301) in water (4 L) were charged to the batch, followed by flushes with water (34 L). The slurry of immobilized GOase$_{Rd13.010}$ in 50 mM pH 8 Bis-Tris was transferred from the filter dryer to the vessel and followed by a flush with water (33 L). The reaction mixture was agitated at 17 °C and sparged with air through a subsurface line (k_La 0.04 s^{-1}). Upon the reaction completion (>90% conv., 21 h, see Figure 5), the batch was transferred to a filter dryer and filtered to remove the immobilized enzyme. The resin wet cake was slurry washed (agitated for 30 mins) twice with water (2 × 63.7 L, 2 × 1 bed volume) and the aqueous solutions were combined to yield a solution of (*R*)-2-ethynylglyceraldehyde 3-phosphate (**3**, 114.2 mol, 83.3% yield, 705.4 kg of a 3.40 wt% solution) that was used directly in the next step.

Pilot plant batch 4 (PPB4): Synthesis of (*R*)-2-ethynylglyceraldehyde 3-phosphate (**3**) using lyophilized immobilized GOase$_{Rd17BB}$

Generation of immobilized lyophilized GOase$_{Rd17BB}$: A slurry of Bio-Rad Nuvia IMAC resin (20 L, 50 vol% in 20% EtOH) was charged to a filter pot and filtered to remove EtOH. The wet cake was slurry washed three times with water (3 × 2.5 bed volumes, 75 L total), followed by a slurry wash with immobilization buffer (2.5 bed volumes, 25 L, 50 mM sodium phosphate, 500 mM NaCl, 15 mM imidazole, pH 8.0). To a jacketed vessel equipped with an overhead stirrer charged with immobilization buffer (11.7 L), copper sulfate pentahydrate (10 g, 1 g per 80 g of enzyme lyophilized powder) was added. The solution was agitated at 230 rpm at room temperature for 1 h until copper sulfate was fully dissolved and GOase$_{Rd17BB}$ (800 g, 6.5 wt% relative to **4**, fit-for purpose fermentation powder) was charged. The enzyme solution was agitated at 116 rpm at room temperature for 1.5 h and then transferred to a jacketed immobilization vessel equipped with an overhead stirrer. The washed slurry of Bio-Rad Nuvia IMAC resin in immobilization buffer (15 L) was transferred to the and aged at 20 °C and 85 rpm for 18h. The resin slurry was transferred to a filter pot and deliquored, was slurry-washed with immobilization buffer (4 × 2.5 bed volumes, 4 × 25 L, 50 mM pH 8 sodium phosphate, 500 mM NaCl, 15 mM pH 8 imidazole), followed by the slurry washes with Bis-Tris methane buffer (4 ×25 L, 50 mM, pH 8.0, total: 200 L, 10 resin bed volumes). The resin was resuspended in Bis-Tris methane buffer (3.3 L, 50 mM, pH 8.0) and transferred into lyophilization trays as a slurry. The enzyme was lyophilized using the following sequence: freeze for 12h at – 40 °C shelf temperature, dry at 450 mT, and a shelf temperature of – 10 °C for 84 h followed by drying at 450 mT and a shelf temperature of 0 °C for 12 h. Lyophilization yielded 1.692 kg of immobilized lyophilized GOase$_{Rd17BB}$ that was stored at -20 °C, prior its use in the oxidation reaction.

Oxidation reaction: (*S*)-2-ethynylglycerol 1-phosphate solution (**4**, 106.8 mol, 248 kg of 8.3 wt% solution) in Bis-Tris methane buffer containing immobilized kinase resin, was charged to a jacketed vessel with jacket, mechanical stirrer, temperature probe, dissolved oxygen sensor, pH probe and air subsurface line and the solution was adjusted to 17 °C. The pH of the reaction mixture was adjusted to pH 7.25 through the addition of 5 M KOH. Catalase from *Corynebacterium glutamicum* (62 g, 0.3 wt% relative to **4**) in water (15 L) and horseradish peroxidase (124 g, 0.6 wt% relative to **4**) in water (15 L) were charged to the batch, followed by immobilized lyophilized GOase$_{Rd17BB}$ resin (2.76 kg, 10.1% water, lyophilized resin containing 200g of GOase$_{Rd17BB}$ powder, 6.5 wt% relative to **4**) and water (135 L). The reaction mixture was agitated at 17 °C and sparged with air through a subsurface line (k_La 0.02 s^{-1}) for 39h. Upon the reaction completion (>90% conv, 39h, see Figure 5), the batch was filtered through a filter dryer to remove the immobilized enzyme. The resin wet cake was washed twice *via* displacement washes with water (2 × 30 L) and the aqueous solutions were combined to yield a solution of (*R*)-2-ethynylglyceraldehyde 3-phosphate (**3**, 92.6 mol, 86.7% yield, 465.3 kg of a 4.18 wt% solution) that was used directly in the next step.

Pilot plant batch 5 (PPB5): Synthesis of (*R*)-2-ethynylglyceraldehyde 3-phosphate (**3**) using non-immobilized GOase$_{Rd17BB}$

Oxidation reaction: In a jacketed vessel water (62 L), copper (II) sulfate pentahydrate (3.6 g, 14.41 mmol, 0.7 wt% relative to GOase$_{Rd17BB}$), and GOase$_{Rd17BB}$ (518 g, 3.6 wt% relative to **4**, optimized fermentation powder) were pre-incubated with agitation at 17 °C for 7.5h. (*S*)-2-ethynylglycerol 1-phosphate solution (**4**, 74.4 mol, 199 kg of 7.2 wt% solution, 14.4 kg,) was charged to a separate jacketed vessel equipped with mechanical stirrer, temperature probe, dissolved oxygen sensor, pH probe and air subsurface line. The solution was cooled to 5 °C and the pH was adjusted to pH 7.1 with 5 M KOH, followed by addition of catalase from *Corynebacterium glutamicum* (43 g, 0.3 wt% relative to **4**) in water (15 L) and horseradish peroxidase (43 g, 0.3 wt% relative to **4**) in water (15 L). The GOase$_{Rd17BB}$ solution was transferred to the vessel containing substrate **4,** followed by a flush with water (10 L). The reaction mixture was agitated at 5 °C and sparged with air through a subsurface line (k_La 0.007 s^{-1}) while maintaining a pressure of 2.9 atm. Upon the reaction completion (>90% conv, 19.5 h, see Figure 5), pressure was released and air sparging stopped to yield a solution of (*R*)-2-ethynylglyceraldehyde 3-phosphate (**3**, 66.8 mol, 89.9% yield, 318.4 kg of a 4.41 wt% solution) was used directly in the next step. ^{1}H NMR (500 MHz, D_2O) δ 5.01 (s, 1H), 3.77 (d, *J* = 11.7 Hz, 1H), 3.73 (d, *J* = 11.7 Hz, 1H), 2.92 (s, 1H). ^{13}C NMR (126 MHz, D_2O) δ 90.3, 81.0, 76.0, 73.9, 65.3.

AUTHOR INFORMATION

Corresponding Author

* (A.F.) anna.fryszkowska@merck.com; (M.H.S) megan.shaw@merck.com

Author Contributions

The manuscript was written through the contributions of all authors. All authors have approved the final version of the manuscript. ‡These authors contributed equally.

Funding Sources

This work was funded by Merck Sharp & Dohme LLC, a subsidiary of Merck & Co., Inc., Rahway, NJ, USA.

Notes

Competing interests: The authors are current or former employees of Merck Sharp & Dohme Corp., a subsidiary of Merck & Co., Inc., Kenilworth, NJ, USA or Codexis, Inc., which are assignees for patents governing chemical matter, processes and enzyme sequences reported in the article: U.S. patent application no. PCT/US2019/040316. Codexis, Inc. has filed patent applications for the evolved enzymes: U.S. patent application nos. PCT/ US2019/040353 (phosphopentomutase), PCT/US2019/040359 (purine nucleoside phosphorylase), PCT/US2019/040369 (aldolase), PCT/US2019/040376 and PCT/US2021/052644 (galactose oxidase), PCT/US2019/040379 (kinase), PCT/US2020/040250 (sucrose phosphorylase), PCT/US2020/040244 (acetate kinase), PCT/US2020/049164 and PCT/2022/0290110 (peroxidase).

ACKNOWLEDGMENT

We acknowledge the help and support of the following people. Merck & Co., Inc., Rahway, NJ, USA team: Mark A. Huffman, Aaron Whittaker, Zhixun Wang, Teresa Andreani for providing supporting data on the performance of the aldol-glycosylation; Joshua Kolev, Niki Patel, Marco Armenante for providing supporting data on the performance of the phosphorylation; Heather Johnson and Shaoguang Zhang for providing supporting data on the chemical and electrochemical oxidation of GOase; Rachel Thatcher for providing support during process characterization; Taylor Behre, Nick Rogus, Travis Armiger for their support of operations at pilot plant scale; Yun Chen for analytical support; Nicholas A. Marshall for support with catalase expression, Amanda Makarewicz for support with oxidase enzyme expression; Brinda Selvaraj for help with submission of crystal structures to PDB; Codexis team: Chris Micklitsch, Alberto Ortega, Auric Sowell-Kantz, Harvinder Maniar, Jessie Slaton, Lilly Miller, Mikayla Krawczyk, Vesna Mitchell, Caroline Selim, Aksiniya Petkova, Nandhitha Subramanian, Nikki Dellas, James Riggins, Jonathan Vroom, Santhosh Sivaramakrishnan, David Entwistle for their support of the directed evolution campaign.

ABBREVIATIONS

API, active pharmaceutical ingredient; DOE, design of experiment; GOase, galactose oxidase; PanK, pantothenate kinase; HRP, horseradish peroxidase; Bis-Tris, Bis-Tris methane buffer; BB – enzyme protein backbone.

ASSOCIATED CONTENT

Supporting Information. Contains detailed procedures for chemistry, molecular biology, enzyme characterization and immobilization; analytical procedures and data; enzyme sequences and crystallization data.

REFERENCES

(1) Huffman, M. A.; Fryszkowska, A.; Alvizo, O.; Borra-Garske, M.; Campos, K. R.; Canada, K. A.; Devine, P. N.; Duan, D.; Forstater, J. H.; Grosser, S. T.; Halsey, H. M.; Hughes, G. J.; Jo, J.; Joyce, L. A.; Kolev, J. N.; Liang, J.; Maloney, K. M.; Mann, B. F.; Marshall, N. M.; McLaughlin, M.; Moore, J. C.; Murphy, G. S.; Nawrat, C. C.; Nazor, J.; Novick, S.; Patel, N. R.; Rodriguez-Granillo, A.; Robaire, S. A.; Sherer, E. C.; Truppo, M. D.; Whittaker, A. M.; Verma, D.; Xiao, L.; Xu, Y.; Yang, H. Design of an in Vitro Biocatalytic Cascade for the Manufacture of Islatravir. *Science (80-.).* **2019**, *366* (6470), 1255–1259. https://doi.org/10.1126/science.aay8484.

(2) Bell, E. L.; Finnigan, W.; France, S. P.; Green, A. P.; Hayes, M. A.; Hepworth, L. J.; Lovelock, S. L.; Niikura, H.; Osuna, S.; Romero, E.; Ryan, K. S.; Turner, N. J.; Flitsch, S. L. Biocatalysis. *Nat. Rev. Methods Prim.* **2021**, *1* (1), 1–21. https://doi.org/10.1038/s43586-021-00044-z.

(3) Dong, J.; Fern, E.; Hollmann, F.; Paul, C. E.; Pesic, M.; Schmidt, S.; Wang, Y.; Younes, S.; Zhang, W. Biocatalytic Oxidation Reactions : A Chemist's Perspective. *Angew. Chemie Int. Ed.* **2018**, *57*, 9238–9261. https://doi.org/10.1002/anie.201800343.

(4) Bong, Y. K.; Song, S.; Nazor, J.; Vogel, M.; Widegren, M.; Smith, D.; Collier, S. J.; Wilson, R.; Palanivel, S. M.; Narayanaswamy, K.; Mijts, B.; Clay, M. D.; Fong, R.; Colbeck, J.; Appaswami, A.; Muley, S.; Zhu, J.; Zhang, X.; Liang, J.; Entwistle, D. Baeyer-Villiger Monooxygenase-Mediated Synthesis of Esomeprazole As an Alternative for Kagan Sulfoxidation. *J. Org. Chem.* **2018**, *83* (14), 7453–7458. https://doi.org/10.1021/acs.joc.8b00468.

(5) Xu, N.; Zhu, J.; Wu, Y.-Q.; Zhang, Y.; Xia, J.-Y.; Zhao, Q.; Lin, G.-Q.; Yu, H.-L.; Xu, J.-H. Enzymatic Preparation of the Chiral (S)-Sulfoxide Drug Esomeprazole at Pilot-Scale Levels. *Org. Process Res. Dev.* **2020**, *24* (6), 1124–1130. https://doi.org/10.1021/acs.oprd.0c00115.

(6) Busch, F.; Brummund, J.; Calderini, E.; Schürmann, M.; Kourist, R. Cofactor Generation Cascade for α-Ketoglutarate and Fe(II)-Dependent Dioxygenases. *ACS Sustain. Chem. Eng.* **2020**. https://doi.org/10.1021/acssuschemeng.0c01122.

(7) Sole, J.; Brummund, J.; Caminal, G.; Gregorio, A.; Schu, M. Enzymatic Synthesis of Trimethyl- ε-Caprolactone: Process Intensif Cation and Demonstration on a 100 L Scale. *Org. Process Res. Dev* **2019**, *23*, 2336−2344. https://doi.org/10.1021/acs.oprd.9b00185.

(8) Schürmann, M. Development and Scale-up of Efficient Biocatalytic Oxidations Using Oxygen EU Horizon2020 Demonstration Workshop : New Developments in Industrial Biocatalysis EU Horizon 2020 Innovation Action " ROBOX " Expanding the Industrial Use of Robust Oxidative Bio. In *EU Horizon2020 demonstration workshop*; 2019.

(9) García-Bofill, M.; Sutton, P. W.; Straatman, H.; Brummund, J.; Schürmann, M.; Guill, M.; Alvaro, G. General Biocatalytic Synthesis of Vanillin by an Immobilised Eugenol Oxidase : High Biocatalyst Yield by Enzyme Recycling. *Appl. Catal. A* **2021**, *General 61*, 117934. https://doi.org/10.1016/j.apcata.2020.117934.

(10) García-Bofill, M.; Sutton, P. W.; Guillén, M.; Álvaro, G. Applied Catalysis A , General Enzymatic Synthesis of Vanillin Catalysed by an Eugenol Oxidase. *Appl. Catal. A, Gen.* **2019**, *582* (June), 117117. https://doi.org/10.1016/j.apcata.2019.117117.

(11) Li, T.; Liang, J.; Ambrogelly, A.; Brennan, T.; Gloor, G.; Huisman, G.; Lalonde, J.; Lekhal, A.; Mijts, B.; Muley, S.; Newman, L.; Tobin, M.; Wong, G.; Zaks, A.; Zhang, X. Efficient, Chemoenzymatic Process for Manufacture of the Boceprevir Bicyclic [3.1.0]Proline Intermediate Based on Amine Oxidase-Catalyzed Desymmetrization. *J. Am. Chem. Soc.* **2012**, *134* (14), 6467–6472. https://doi.org/10.1021/ja3010495.

(12) Archer, I. V. J.; Fotheringham, I.; Carr, R.; Arnold, S. A. Stereoinversion of Amino Acids in a Single Reactor US8133717B2. US8133717B2, 2012.

(13) Taylor, P. P.; Speight, R. E. Compositions of Variant Biocatalysts for Preparing Enantiopure Amino Acids US20110059503A1. US20110059503A1, 2011. https://doi.org/10.1111/2047-8852.12112.

(14) Bartsch, S.; Brummund, J.; Köpke, S.; Straatman, H.; Vogel, A.; Schürmann, M. Optimization of Alcohol Dehydrogenase for Industrial Scale Oxidation of Lactols. *Biotechnol. J.* **2020**, *2000171*, 1–13. https://doi.org/10.1002/biot.202000171.

(15) Goundry, W. R. F.; Adams, B.; Benson, H.; Demeritt, J.; Mckown, S.; Mulholland, K.; Robertson, A.; Siedlecki, P.; Tomlin, P.; Vare, K. Development and Scale-up of a Biocatalytic Process To Form a Chiral Sulfoxide. *Org. Process Res. Dev.* **2017**, *21*, 107–113. https://doi.org/10.1021/acs.oprd.6b00391.

(16) Goundry, W. R. F.; Dai, K.; Gonzalez, M.; Legg, D.; O'Kearney-Mcmullan, A.; Morrison, J.; Stark, A.; Siedlecki, P.; Tomlin, P.; Yang, J. Development and Scale-up of a Route to ATR Inhibitor AZD6738. *Org. Process Res. Dev.* **2019**, *23* (7), 1333–1342. https://doi.org/10.1021/acs.oprd.9b00075.

(17) Graham, M. A.; Askey, H.; Campbell, A. D.; Chan, L.; Cooper, K. G.; Cui, Z.; Dalgleish, A.; Dave, D.; Ensor, G.; Rita, M.; Espinosa, G.; Hamilton, P.; He, C.; Jackson, L. V; Jing, D.; Jones, M. F.; Liu, P.; Mulholland, K. R.; Pervez, M.; Popadynec, M.; Randles, E.; Tomasi, S.; Wang, S. Development and Scale-Up of an Improved Manufacturing Route to the ATR Inhibitor Ceralasertib. *Org. Process Res. Dev. 2021*, **2021**, *25*, 43–56. https://doi.org/10.1021/acs.oprd.0c00482.

(18) Toftgaard Pedersen, A.; Birmingham, W. R.; Rehn, G.; Charnock, S. J.; Turner, N. J.; Woodley, J. M. Process Requirements of Galactose Oxidase Catalyzed Oxidation of Alcohols. *Org. Process Res. Dev.* **2015**, *19* (11), 1580–1589. https://doi.org/10.1021/acs.oprd.5b00278.

(19) Birmingham, W. R.; Pedersen, A. T.; Gomes, M. D.; Madsen, M. B.; Breuer, M.; Woodley, J. M.; Turner, N. J. Toward Scalable Biocatalytic Conversion of 5-Hydroxymethylfurfural by Galactose Oxidase Using Coordinated Reaction and Enzyme Engineering. *Nat. Commun.* **2021**, *12*, 4946. https://doi.org/10.1038/s41467-021-25034-3.

(20) McIntosh, J. A.; Benkovics, T.; Silverman, S. M.; Huffman, M. A.; Kong, J.-R.; Maligres, P. E.; Itoh, T.; Yang, H.; Verma, D.; Pan, W.; Ho, H. I.; Vroom, J.; Knight, A. M.; Hurtak, J. A.; Klapars, A.; Fryszkowska, A.; Morris, W. J.; Strotman, N. A.; Murphy, G. S.; Maloney, K. M.; Fier, P. S. Engineered Ribosyl-1-Kinase Enables Concise Synthesis of Molnupiravir, an Antiviral for COVID-19. *ACS Cent. Sci.* **2021**, *7* (12), 1980–1985. https://doi.org/10.1021/acscentsci.1c00608.

(21) Kaluzna, I.; Schmitges, T.; Straatman, H.; van Tegelen, D.; Müller, M.; Schürmann, M.; Mink, D. Enabling Selective and Sustainable P450 Oxygenation Technology. Production of 4-Hydroxy-α-Isophorone on Kilogram Scale. *Org. Process Res. & Dev.* **2016**, *20* (4), 814–819. https://doi.org/10.1021/acs.oprd.5b00282.

(22) Brummund, J.; Müller, M.; Schmitges, T.; Kaluzna, I.; Mink, D.; Hilterhaus, L.; Liese, A. Process Development for Oxidations of Hydrophobic Compounds Applying Cytochrome P450 Monooxygenases In-Vitro. *J. Biotechnol.* **2016**, *233*, 143–150. https://doi.org/10.1016/j.jbiotec.2016.07.002.

(23) Truppo, M. D. Biocatalysis in the Pharmaceutical Industry: The Need for Speed. *ACS Med. Chem. Lett.* **2017**, *8* (5), 476–480. https://doi.org/10.1021/acsmedchemlett.7b00114.

(24) Woodley, J. M. Integrating Protein Engineering with Process Design for Biocatalysis. *Philos. Trans. R. Soc. A Math. Phys. Eng. Sci.* **2018**, *376* (2110). https://doi.org/10.1098/rsta.2017.0062.

(25) McIntosh, J. A.; Owens, A. E. Enzyme Engineering for Biosynthetic Cascades. *Curr. Opin. Green Sustain. Chem.* **2021**, *29*, 100448. https://doi.org/10.1016/j.cogsc.2021.100448.

(26) Fryszkowska, A.; Devine, P. N. Biocatalysis in Drug Discovery and Development. *Curr. Opin. Chem. Biol.* **2020**, *55* (April), 151–160. https://doi.org/10.1016/j.cbpa.2020.01.012.

(27) Barrett, S. E.; Teller, R. S.; Forster, S. P.; Li, L.; Mackey, M. A.; Skomski, D.; Yang, Z.; Fillgrove, K. L.; Doto, G. J.; Wood, S. L.; Lebron, J.; Grobler, J. A.; Sanchez, R. I.; Liu, Z.; Lu, B.; Niu, T.; Sun, L.; Gindy, M. E. Extended-Duration MK-8591-Eluting Implant as a Candidate for HIV Treatment and Prevention. *Antimicrob. Agents Chemother.* **2018**, *62* (10), 1–13. https://doi.org/10.1128/AAC.01058-18.

(28) Rummelt, S. M.; Qi, J.; Chen, Y.; Dropinski, J. F.; Hughes, G.; Jeffrey, T.; Li, D.; Maloney, K. M.; Margelefsky, E.; Mathew, R.; Muzzio, D. J.; Nawrat, C. C.; Newman, J. A.; Ouyang, H.; Patel, N. R.; Qiao, Z.; Sirota, E.; Song, Z. J.; Tan, L.; Varsolona, R. J.; Wan, B.; Brian, M.; Xu, F.; Xu, Y.; Yin, J.; Zhang, S.; Zhao, R. Development of an Efficient Route to 2-Ethynylglycerol for the Synthesis of Islatravir. *ChemRxiv* **2021**. https://doi.org/10.26434/chemrxiv.14502744.v1.

(29) Fier, P. S.; Shaw, M. H. Biocatalytic Syntheses of Antiviral Nucleosides Islatravir and Molnupiravir. In *Reference Collection in Chemistry, Molecular Sciences and Chemical Engineering*; Elsevier, 2022. https://doi.org/https://doi.org/10.1016/B978-0-32-390644-9.00047-0.

(30) Patel, N. R.; Kolev, J. N.; Fryszkowska, A. Development of a Kinase-Catalyzed Phosphorylation and ATP Recycling System for the Synthesis of Islatravir (Manuscript in Preparation).

(31) Mattern, K.; Grosser, S. T. Automated End-to-End Workflow for Volumetric Mass-Transfer Coefficient (kLa) Characterization in Small-Molecule Pharmaceutical Development. *Org. Process Res. Dev.* **2023**. https://doi.org/10.1021/acs.oprd.3c00191.

(32) Attadgie, I.; Mattern, K. Achieving Optimal Oxygen Mass Transfer for Aerobic Biocatalytic Oxidations in Small Molecule Process Development (Manuscript in Preparation).

(33) Xu, K.; Chen, X.; Zheng, R.; Zheng, Y. Immobilization of Multi-Enzymes on Support Materials for Efficient Biocatalysis. **2020**, *8* (June), 1–17. https://doi.org/10.3389/fbioe.2020.00660.

(34) Whittaker, A. M.; Miller, M.; Kwok, T. T.; Huffman, M.; Wang, Z.; An-, T.; Dobson, B.; Gunsch, M.; Sirota, E.; Mattern, K.; Mohan, A.; Heltzel, J.; Lamberto, D. J.; Harbor, V.; Rosenthal, R.; Xu, Y.; Margelefsky, E.; Robaire, S.; Hughes, G.; Maloney, K.; Campeau, L. C.; Campos, K. Development of a 4-Enzyme Biocatalytic Aldol-Glycosylation Cascade for the Product Forming Step of the Islatravir Manufacturing Route (Manuscript in Preparation).

(35) Chen, Y.; Jo, J.; Hernandez, E.; Wang, H.; Bernardoni, F. Biocatalytic Cascade Process of Islatravir: Analytical and Regulatory Control Strategy of Minor Enantiomer. *J. Pharm. Biomed. Anal.* **2023**, *234* (May), 115536. https://doi.org/10.1016/j.jpba.2023.115536.

(36) Ouimet, C. M.; Foley, D. A.; Hughes, G.; Pilo, A. L.; Schwalm, E. L.; Jo, J.; Chen, Y. A Total Protein HPLC Assay for Residual Protein Control in Islatravir Synthesized by Biocatalysis (Manuscript in Preparation).

(37) Gunsch, M. J.; Schwalm, E. L.; Ouimet, C. M.; Halsey, H. M.; Hamilton, S. E.; Bernardoni, F.; Jo, J. Development and Validation of Ion-Pairing HPLC-CAD Chromatography for Measurement of Islatravir's Phosphorylated Intermediates. *J. Pharm. Biomed. Anal.* **2022**, *213* (January), 114684. https://doi.org/10.1016/j.jpba.2022.114684.

(38) Fier, P. S.; Xu, Y.; Poirier, M.; Brito, G.; Zheng, M.; Bade, R.; Sirota, E.; Stone, K.; Tan, L.; Humphrey, G. R.; Chang, D.; Bothe, J.; Zhang, Y.; Bernardoni, F.; Castro, S.; Zompa, M. A.; Taylor, J.; Sirk, K. M.; Diaz-Santana, A.; Diribe, I.; Emerson, K. M.; Krishnamurthi, B.; Zhao, R.; Ward, M.; Xiao, C.; Ouyand, H.; Zhan, J.; Morris, W. J. Development of a Robust Manufacturing Route for Molnupiravir, an Antiviral for the Treatment of COVID-19. *Org. Process Res. Dev.* **2021**. https://doi.org/10.1021/acs.oprd.1c00400.

(39) Whittaker, J. W. Free Radical Catalysis by Galactose Oxidase. *Chem. Rev.* **2003**, *103* (6), 2347–2364. https://doi.org/10.1021/cr020425z.

(40) Johnson, H. C.; Zhang, S.; Fryszkowska, A.; Ruccolo, S.; Robaire, S. A.; Klapars, A.; Patel, N. R.; Whittaker, A. M.; Huffman, M. A.; Strotman, N. A. Biocatalytic Oxidation of Alcohols Using Galactose Oxidase and a Manganese(Iii) Activator for the Synthesis of Islatravir. *Org. Biomol. Chem.* **2021**, *19* (7), 1620–1625. https://doi.org/10.1039/d0ob02395g.

(41) Zhang, S.; Ruccolo, S.; Fryszkowska, A.; Klapars, A.; Marshall, N.; Strotman, N. A. Electrochemical Activation of Galactose Oxidase: Mechanistic Studies and Synthetic Applications. *ACS Catal.* **2021**, *11*, 7270–7280. https://doi.org/10.1021/acscatal.1c01037.

(42) Rogers, M. S.; Tyler, E. M.; Akyumani, N.; Kurtis, C. R.; Spooner, R. K.; Deacon, S. E.; Tamber, S.; Firbank, S. J.; Mahmoud, K.; Knowles, P. F.; Phillips, S. E. V; McPherson, M. J.; Dooley, D. M. The Stacking Tryptophan of Galactose Oxidase: A Second-Coordination Sphere Residue That Has Profound Effects on Tyrosyl Radical Behavior and Enzyme. *Biochemistry* **2007**, No. Figure 1, 4606–4618. https://doi.org/10.1021/bi062139d.

(43) Borra-Garske, M. T.; Nazor, J.; Subramanian, N.; Alvizo, O.; Fryszkowska, A. WO/2022/076263 A1 Engineered Galactose Oxidase Variant Enzymes, 2022.

(44) Sun, L.; Petrounia, I. P.; Yagasaki, M.; Bandara, G.; Arnold, F. H. Expression and Stabilization of Galactose Oxidase in Escherichia Coli by Directed Evolution. *Protein Eng. Des. Sel.* **2001**, *14* (9), 699–704. https://doi.org/10.1093/protein/14.9.699.

(45) Rogers, M. S.; Hurtado-Guerrero, R.; Firbank, S. J.; Halcrow, M. A.; Dooley, D. M.; Phillips, S. E. V.; Knowles, P. F.; McPherson, M. J. Cross-Link Formation of the Cysteine 228-Tyrosine 272 Catalytic Cofactor of Galactose Oxidase Does Not Require Dioxygen. *Biochemistry* **2008**, *47* (39), 10428–10439. https://doi.org/10.1021/bi8010835.

(46) Whittaker, M. M.; Whittaker, J. W. Cu(I)-Dependent Biogenesis of the Galactose Oxidase Redox Cofactor. *J. Biol. Chem.* **2003**, *278* (24), 22090–22101. https://doi.org/10.1074/jbc.M300112200.

(47) Kwiatkowski, L. D.; Adelman, M.; Pennelly, R.; Kosman, D. J. Kinetic Mechanism of the Cu(II) Enzyme Galactose Oxidase. *J. Inorg. Biochem.* **1981**, *14* (3), 209–222. https://doi.org/10.1016/S0162-0134(00)80001-X.

(48) Roncal, T.; Muñoz, C.; Lorenzo, L.; Maestro, B.; Díaz de Guereñu, M. del M. Two-Step Oxidation of Glycerol to Glyceric Acid Catalyzed by the Phanerochaete Chrysosporium Glyoxal Oxidase. *Enzyme Microb. Technol.* **2012**, *50* (2), 143–150. https://doi.org/10.1016/j.enzmictec.2011.11.007.

(49) Wohlschlager, L.; Kracher, D.; Scheiblbrandner, S.; Csarman, F.; Ludwig, R. Spectroelectrochemical Investigation of the Glyoxal Oxidase Activation Mechanism. *Bioelectrochemistry* **2021**, *141*, 107845. https://doi.org/10.1016/j.bioelechem.2021.107845.

(50) Forget, S.; Xia, R. (Fan); Hein, J. E.; Brumer, H. Determination of Biocatalytic Parameters of a Copper Radical Oxidase Using Real-Time Reaction Progress Monitoring. *Org. Biomol. Chem.* **2020**. https://doi.org/10.1039/c9ob02757b.

(51) Tressel, P.; Kosman, D. J. O,O-Dityrosine in Native and Horseradish Peroxidase-Activated Galactose Oxidase. *Biochem. Biophys. Res. Commun.* **1980**, *92* (3), 781–786.

(52) Sato, S.; Matsumura, M.; Kadonosono, T.; Abe, S.; Ueno, T.; Ueda, H.; Nakamura, H.; Sato, S.; Nakamura, H. Site-Selective Protein Chemical Modification of Exposed Tyrosine Residues Using Tyrosine Click Reaction. *Bioconjug. Chem.* **2020**, *31* (5), 1417–1424. https://doi.org/10.1021/acs.bioconjchem.0c00120.

(53) Minamihata, K.; Goto, M.; Kamiya, N. Site-Specific Conjugation of an Antibody-Binding Protein Catalyzed by Horseradish Peroxidase Creates a Multivalent Protein Conjugate with High Affinity to IgG. *Biotechnol. J.* **2015**, *10* (1), 222–226. https://doi.org/10.1002/biot.201400512.

(54) Gray, H. B.; Winkler, J. R. Living with Oxygen. *Acc. Chem. Res.* **2018**, *51* (8), 1850–1857. https://doi.org/10.1021/acs.accounts.8b00245.

(55) Gray, H. B.; Winkler, J. R. Hole Hopping through Tyrosine/Tryptophan Chains Protects Proteins from Oxidative Damage. *Proc. Natl. Acad. Sci. U. S. A.* **2015**, *112* (35), 10920–10925. https://doi.org/10.1073/pnas.1512704112.

(56) Da Duan; Sowell-Kantz, A. A.; Aksiniya, P.; Nazor, J.; Subramanian, N.; Alvizo; Duan, D.; Sowell-Kantz, A. A.; Petkova, A. L.; Nazor, J.; Subramanian, N.; Alvizo, O. Peroxidase Activity towards 10-Acetyl-3,7-Dihydroxyphenoxazine PCT/US2022/0290110. WO2021050348A1, 2022.

(57) Passardi, F.; Cosio, C.; Penel, C.; Dunand, C. Peroxidases Have More Functions than a Swiss Army Knife. *Plant Cell Rep.* **2005**, *24* (5), 255–265. https://doi.org/10.1007/s00299-005-0972-6.

(58) Sirota, E.; Kwok, T.; Varsolona, R. J.; Whittaker, A.; Andreani, T.; Quirie, S.; Margelefsky, E.; Lamberto, D. J. Crystallization Process Development for the Final Step of the Biocatalytic Synthesis of Islatravir : Comprehensive Crystal Engineering for a Low-Dose Drug. *Org. Process Res. Dev.* **2021**, *25*, 308–317. https://doi.org/10.1021/acs.oprd.0c00520.

(59) Romero-Fernández, M.; Paradisi, F. Protein Immobilization Technology for Flow Biocatalysis. *Curr. Opin. Chem. Biol.* **2020**, *55*, 1–8. https://doi.org/10.1016/j.cbpa.2019.11.008.

(60) Thompson, M. P.; Derrington, S. R.; Heath, R. S.; Porter, J. L.; Mangas-Sanchez, J.; Devine, P. N.; Truppo, M. D.; Turner, N. J. A Generic Platform for the Immobilisation of Engineered Biocatalysts. *Tetrahedron* **2019**, *75* (3), 327–334. https://doi.org/10.1016/j.tet.2018.12.004.

(61) Boudrant, J.; Woodley, J. M.; Fernandez-Lafuente, R. Parameters Necessary to Define an Immobilized Enzyme Preparation. *Process Biochem.* **2020**, *90* (November 2019), 66–80. https://doi.org/10.1016/j.procbio.2019.11.026.

(62) Forstater, J. H.; Grosser, S. T. Data-Rich Process Development of Immobilized Biocatalysts in Flow. *React. Chem. Eng.* **2021**. https://doi.org/10.1039/D1RE00298H.

(63) Ringborg, R. H.; Toftgaard Pedersen, A.; Woodley, J. M. Automated Determination of Oxygen-Dependent Enzyme Kinetics in a Tube-in-Tube Flow Reactor. *ChemCatChem* **2017**, *9* (17), 3285–3288. https://doi.org/10.1002/cctc.201700811.

(64) Lara, M.; Mutti, F. G.; Glueck, S. M.; Kroutil, W. Biocatalytic Cleavage of Alkenes with O2 and Trametes Hirsuta G FCC 047. *European J. Org. Chem.* **2008**, No. 21, 3668–3672. https://doi.org/10.1002/ejoc.200800261.

(65) Chapman, A. M. R.; Cosgrove, S. C.; Nicholas, J.; Kapur, N.; Blacker, A. J.; Chapman, M. R.; Cosgrove, S. C.; Turner, N. J.; Kapur, N.; Blacker, A. J.; Chapman, A. M. R.; Cosgrove, S. C.; Nicholas, J.; Kapur, N.; Blacker, A. J. Highly Productive Oxidative Biocatalysis in Continuous-Flow by Surpassing the Aqueous Equilibrium Solubility of Oxygen. *Angew. Chemie Int. Ed.* **2018**, 2–7. https://doi.org/10.1002/anie.201803675.

(66) Lee, T. M.; Qian, S.; Fisher, B. F.; Downing, S.; Chakrabarti, G.; Hunt, S. Compositions and Methods for Production of Glucose Oxidation Products WO2021178935A1. WO2021178935A1, 2021.

(67) Davis, S. C.; Huisman, G. W.; Jenne, S. J.; Krebber, A.; Newman, L. M. Ketoreductase Polypeptides and Related Polynucleotides US2006/0195947 A1. US 2006/0195947 A1, 2006.

(68) Huffman, M. A.; Fryszkowska, A.; Kolev, J. N.; Devine, P. N.; Campos, K. R.; Truppo, M. D.; Nawrat, C. C. Enzymatic Synthesis of 4'-Ethynyl Nucleoside Analogs WO 2020/014041 A1. WO 2020/014041 A1, 2020.

(69) McIntosh, J. A.; Liu, Z.; Andresen, B. M.; Marzijarani, N. S.; Moore, J. C.; Marshall, N. M.; Borra-Garske, M.; Obligacion, J. V.; Fier, P. S.; Peng, F.; Forstater, J. H.; Winston, M. S.; An, C.; Chang, W.; Lim, J.; Huffman, M. A.; Miller, S. P.; Tsay, F. R.; Altman, M. D.; Lesburg, C. A.; Steinhuebel, D.; Trotter, B. W.; Cumming, J. N.; Northrup, A.; Bu, X.; Mann, B. F.; Biba, M.; Hiraga, K.; Murphy, G. S.; Kolev, J. N.; Makarewicz, A.; Pan, W.; Farasat, I.; Bade, R. S.; Stone, K.; Duan, D.; Alvizo, O.;

Adpressa, D.; Guetschow, E.; Hoyt, E.; Regalado, E. L.; Castro, S.; Rivera, N.; Smith, J. P.; Wang, F.; Crespo, A.; Verma, D.; Axnanda, S.; Dance, Z. E. X.; Devine, P. N.; Tschaen, D.; Canada, K. A.; Bulger, P. G.; Sherry, B. D.; Truppo, M. D.; Ruck, R. T.; Campeau, L. C.; Bennett, D. J.; Humphrey, G. R.; Campos, K. R.; Maddess, M. L. A Kinase-CGAS Cascade to Synthesize a Therapeutic STING Activator. *Nature* **2022**, *603* (7901), 439–444. https://doi.org/10.1038/s41586-022-04422-9.

(70) Micklitsch, C. M.; Alvizo, O.; Nazor, J.; Maniar, H. C.; Krawczyk, M. J.; Borra-Garske, M. T.; Subramanian, N.; Fryszkowska, A.; Marshall, N. M.; Rodriguez-Granillo, A.; Verma, D.; Andrews, D. Engineered Galactose Oxidase Variant Enzymes WO 2020/014049 A1. WO 2020/014049 A1, 2020.

(71) Notredame, C.; Higgins, D. G.; Heringa, J. T-Coffee: A Novel Method for Fast and Accurate Multiple Sequence Alignment. *J. Mol. Biol.* **2000**, *302* (1), 205–217. https://doi.org/https://doi.org/10.1006/jmbi.2000.4042.

(72) Bricogne, G.; Blanc, E.; Brandl, M.; Flensburg, C.; Keller, P.; Paciorek, W.; Roversi, P.; Sharff, A.; Smart, O.; Vonrhein, C.; Womack, T. BUSTER v.2.11.6. Http://Www.Globalphasing.Com. 2018.

(73) Winn, M. D.; Ballard, C. C.; Cowtan, K. D.; Dodson, E. J.; Emsley, P.; Evans, P. R.; Keegan, R. M.; Krissinel, E. B.; Leslie, A. G. W.; McCoy, A.; McNicholas, S. J.; Murshudov, G. N.; Pannu, N. S.; Potterton, E. A.; Powell, H. R.; Read, R. J.; Vagin, A.; Wilson, K. S. Overview of the CCP4 Suite and Current Developments. *Acta Crystallogr. Sect. D Biol. Crystallogr.* **2011**, *67* (4), 235–242. https://doi.org/10.1107/S0907444910045749.

(74) Rannes, J. B.; Ioannou, A.; Willies, S. C.; Grogan, G.; Behrens, C.; Flitsch, S. L.; Turner, N. J. Glycoprotein Labeling Using Engineered Variants of Galactose Oxidase Obtained by Directed Evolution. *J. Am. Chem. Soc* **2011**, *133*, 8436–8439. https://doi.org/10.1021/ja2018477.

(75) P. Emsley; Lohkamp, B.; Scott, W. G.; Cowtan, K. Features and Development of Coot. *Acta Crystallogr. Sect. D Biol. Crystallogr.* **2010**, *66*, 486–501.